TITLE

An important role for triglyceride in regulating spermatogenesis

AUTHORS

Charlotte F. Chao[1&], Yanina-Yasmin Pesch[1&], Huaxu Yu[2], Chenjingyi Wang[2], Maria Aristizabal[3], Tao Huan[2], Guy Tanentzapf[1], Elizabeth J. Rideout[1*]

AFFILIATIONS

[1] Department of Cellular and Physiological Sciences, Life Sciences Institute, The University of British Columbia, Vancouver, BC, Canada V6T 1Z3

[2] Department of Chemistry, The University of British Columbia, Vancouver, BC, Canada V6T 1Z1

[3] Department of Biology, Queen's University, Kingston, ON, Canada K7L 3N6

* Corresponding author

[&] Equally contributing authors

[*] Correspondence: elizabeth.rideout@ubc.ca

ABSTRACT

Drosophila is a powerful model to study how lipids affect spermatogenesis. Yet, the contribution of neutral lipids, a major lipid group which resides in organelles called lipid droplets (LD), to normal sperm development is largely unknown. Emerging evidence suggests that LD are present in the testis and that loss of neutral lipid- and LD-associated genes causes subfertility; however, key regulators of testis neutral lipids and LD remain unclear. Here, we show that LD are present in early-stage somatic and germline cells within the *Drosophila* testis. We identified a role for triglyceride lipase *brummer* (*bmm*) in regulating testis LD, and found that whole-body loss of *bmm* leads to defects in sperm development. Importantly, these represent cell-autonomous roles for *bmm* in regulating testis LD and spermatogenesis. Because lipidomic analysis of *bmm* mutants revealed excess triglyceride accumulation, and spermatogenic defects in *bmm* mutants were rescued by genetically blocking triglyceride synthesis, our data suggest that *bmm*-mediated regulation of triglyceride influences sperm development. This identifies triglyceride as an important neutral lipid that contributes to *Drosophila* sperm development, and reveals a key role for *bmm* in regulating testis triglyceride levels during spermatogenesis.

KEYWORDS

Triglyceride, lipid droplet, spermatogenesis, testis, *brummer*, adipose triglyceride lipase (ATGL), lipidomics.

INTRODUCTION

Lipids play an essential role in regulating spermatogenesis across animals [1–4]. Studies in *Drosophila* have illuminated key roles for multiple lipid species in regulating sperm development [5–7]. For example, phosphatidylinositol and its phosphorylated derivatives participate in diverse aspects of *Drosophila* spermatogenesis including meiotic cytokinesis [1,8–11], somatic cell differentiation [12], germline and somatic cell polarity maintenance [13–16], and germline stem cell (GSC) maintenance and proliferation [17]. Membrane lipids also influence sperm development [18,19], whereas fatty acids play a role in processes such as meiotic cytokinesis [20] and sperm individualization [21,22]. While these studies suggest key roles for membrane lipids and fatty acids during *Drosophila* spermatogenesis, some of which are conserved in mammals [23–25], much less is known about how neutral lipids contribute to spermatogenesis.

Neutral lipids are a major lipid group that includes triglyceride and cholesterol ester, and reside within specialized organelles called lipid droplets (LD) [26]. LD are found in diverse cell types (*e.g*. adipocytes, muscle, liver, glia, neurons) [27,28,26], and play key roles in maintaining cellular lipid homeostasis. In nongonadal cell types, correct regulation of LD contributes to cellular energy production [29–31], sequestration and redistribution of lipid precursors [32–36], and regulation of lipid toxicity [37–39]. The importance of LD to normal cellular function in nongonadal cell types is shown by the fact that dysregulation of LD causes defects in cell differentiation, survival, and energy production [26,37,40,41]. In the testis, much less is known about the regulation and function of neutral lipids and LD, and how this regulation affects sperm development.

62 Multiple lines of evidence suggest a potential role for neutral lipids and LD during
63 spermatogenesis. First, genes that encode proteins associated with neutral lipid
64 metabolism and LD are expressed in the testis across multiple species [42–44].
65 Second, testis LD have been identified in mammals and flies under both normal
66 physiological conditions [27,44–48] and after mitochondrial stress [49]. Third, loss of
67 genes associated with neutral lipid metabolism and LD cause subfertility phenotypes in
68 both flies and mammals [27,50–52]. While studies suggest that mammalian testis LD
69 contribute to steroidogenesis [53,54], the spatial, temporal, and cell-type specific
70 requirements for neutral lipids and LD in the testis have not been explored in detail in
71 any animal. It remains similarly unclear which genes are responsible for regulating
72 neutral lipids and LD during spermatogenesis.
73 To address these knowledge gaps, we used *Drosophila* to investigate the
74 regulation and function of neutral lipids and LD during sperm development. Our detailed
75 analysis of spermatogenesis under normal physiological conditions revealed the
76 presence of LD in early-stage somatic and germline cells in the testis. We identified
77 triglyceride lipase *brummer* (*bmm*) as a regulator of testis LD, and showed that this
78 represents a cell-autonomous role for *bmm*. Importantly, we found that the *bmm*-
79 mediated regulation of testis LD was significant for spermatogenesis, as both whole-
80 body and cell-autonomous loss of *bmm* caused defects in sperm development. Given
81 that our lipidomic analysis revealed an excess accumulation of triglyceride in animals
82 lacking *bmm*, and that genetically blocking triglyceride synthesis rescued many
83 spermatogenic defects associated with *bmm* loss, our data suggests that *bmm*-
84 mediated regulation of triglyceride is important for normal *Drosophila* sperm

85 development. This reveals previously unrecognized roles for neutral lipids such as
86 triglyceride in regulating spermatogenesis, and for *bmm* in regulating sperm
87 development under normal physiological conditions. Together, these findings advance
88 knowledge of the regulation and function of neutral lipids during spermatogenesis.
89

90 **RESULTS**

91 **Lipid droplets are present in early-stage somatic and germline cells**

92 We previously reported the presence of small circular punctae (<1 μm) corresponding to
93 LD near the apical tip of the testis [27]. We confirm these results in w^{1118} males using
94 neutral lipid stain BODIPY (4,4-Difluoro-1,3,5,7,8-Pentamethyl-4-Bora-3a,4a-Diaza-*s*-
95 Indacene) (Figure 1A). Importantly, we reproduced this spatial distribution of LD in two
96 independent genetic backgrounds and at two additional ages (Figure 1B,1C). In all
97 cases, LD were in a testis region that contains stem cells and early-stage somatic and
98 germline cells (Figure 1A-A', arrows), and in the hub, an organizing center and stem cell
99 niche in the *Drosophila* testis (Figure 1A''-A''', arrows) [55]. LD were largely absent from
100 the testis region occupied by spermatocytes (Figure 1A and A', arrowheads). While LD
101 may contain multiple neutral lipid species[56], cholesterol-binding fluorescent polyene
102 antibiotic filipin III did not detect cholesterol within testis LD (Figure S1A), suggesting
103 triglyceride is the main neutral lipid in *Drosophila* testis LD.

104 *Drosophila* spermatogenesis requires the codevelopment and differentiation of
105 two cell lineages, the germline and the somatic cells [57]. To identify LD in each lineage,
106 we used the GAL4/UAS system to overexpress a transgene in which GFP is fused to
107 the LD-targeting motif of motor protein Klarsicht [58] (*UAS-GFP-LD*). We targeted *UAS-*

108 *GFP-LD* to somatic cells with *Traffic jam* (*Tj*)-*GAL4* and to the germline using *nanos*
109 *(nos)-GAL4*; LD were visualized using neutral lipid dye LipidTox. We found LD in the
110 somatic cells of 0-day-old males (Figure 1D), and showed that the majority of somatic
111 LD were <30 μm from the hub (Figure 1E). Because the somatic LD distribution
112 coincided with a marker for somatic stem cells and their immediate daughter cells (Zinc
113 finger homeodomain 1, Zfh-1) (Figure 1F; two-sample Kolmogorov-Smirnov test) [59],
114 but not with a marker for late somatic cells (Eyes absent, Eya) [12,60], our data
115 suggests LD are present in early somatic cells. In the germline, GFP punctae
116 corresponding to LD were found near the apical tip of the testis in 0-day-old males
117 (Figure 1G,H). We found that the disappearance of germline LD coincided with peak
118 expression of a GFP reporter that reflects the expression of Bag-of-marbles (Bam)
119 protein in the testis (Bam-GFP) [61] (Figure 1I,1J). Because peak Bam expression
120 signals the last round of transient amplifying mitotic cell cycle prior to the germline's
121 transition into the meiotic cell cycle [62–64], our data suggests that germline LD, like
122 somatic LD, are present at early stages of germline development.
123

124 ***brummer* plays a cell-autonomous role in regulating testis lipid droplets**

125 *Adipose triglyceride lipase* (*ATGL*) is a critical regulator of neutral lipid metabolism and
126 LD [65–74]. Loss of *ATGL* in many cell types triggers LD accumulation, and *ATGL*
127 overexpression decreases LD number [30,67,68,71,73,73,75,76]. Given that the
128 *Drosophila ATGL* homolog *brummer* (*bmm*) regulates testis LD induced by
129 mitochondrial stress [49], we explored whether *bmm* regulates testis LD under normal
130 physiological conditions. We first examined *bmm* expression in the testis by isolating

131 this organ from flies in which a *bmm* promoter fragment drives *GFP* expression (*bmm-*
132 *GFP*). Indeed, *bmm-GFP* accurately reproduces changes to *bmm* mRNA levels [77].
133 GFP expression was present in the germline of *bmm-GFP* testes, and we found
134 germline GFP levels were higher in spermatocytes than at earlier stages of sperm
135 development (Figure 2A,2B; one-way ANOVA with Tukey multiple comparison test).
136 Supporting this, our analysis of a publicly available single-cell RNA sequencing data set
137 of the male reproductive organ [78] suggested a similar trend in *bmm* mRNA levels
138 between different stages of germline (Figure S2A,S2B) and somatic cell (Figure
139 S2C,S2D) development. Importantly, germline GFP levels were negatively correlated
140 with testis LD in *bmm-GFP* flies (Figure 2A,2C), suggesting regions with higher *bmm*
141 expression had fewer LD.

142 To test whether *bmm* regulates testis LD, we compared LD in testes from 0-day-
143 old males carrying a loss-of-function mutation in *bmm* (bmm^{1}) to control male testes
144 (bmm^{rev})[67]. bmm^{1} testes had significantly more LD across all LD sizes compared with
145 control males (Figure 2D–2G; Welch two-sample t-test with Bonferroni correction), and
146 showed a significantly expanded LD distribution (Figure 2D–2F,2H; two-sample
147 Kolmogorov-Smirnov test). This suggests *bmm* normally restricts LD to the region near
148 the apical tip of the testis, a role we confirm in both somatic and germline lineages
149 (Figure S2E–S2H). Importantly, after inducing homozygous bmm^{1} or bmm^{rev} clones in
150 the testes using *FLP-FRT* system[79], we found bmm^{1} spermatocyte clones had
151 significantly more LD at 3 days post-clone induction (Figure 2I; Welch two-sample t-
152 test), a stage at which LD were absent from bmm^{rev} clones. This indicates a previously

153 unrecognized cell-autonomous role for *bmm* in regulating testis LD, a role we were
154 unable to assess in somatic cells as we recovered no *bmm*^{1} somatic cell clones.
155
156 ***brummer* plays a cell-autonomous role in regulating germline development**
157 To determine the physiological significance of *bmm*-mediated regulation of testis LD, we
158 investigated testis and sperm development in males without *bmm* function. In 0-day-old
159 *bmm*^{1} males reared at 25°C, testis size was significantly smaller than in age-matched
160 *bmm*^{rev} controls (Figure S3A; Welch two-sample t-test), and the number of spermatid
161 bundles was significantly lower (Figure S3B; Kruskal-Wallis rank sum test). Defects in
162 testis size and sperm development were also observed in 14-day-old *bmm*^{1} males
163 (Figure S3C,S3D Welch two-sample t-test). When the animals were reared at 29°C, a
164 temperature that exacerbates spermatogenesis defects associated with changes in lipid
165 metabolism [21], *bmm*^{1} phenotypes were more pronounced (Figure 3A-3C). This
166 suggests loss of *bmm* affects testis development and spermatogenesis. Because similar
167 phenotypes are observed in male mice without ATGL [52], and supplementing the diet
168 of *bmm*^{1} males with medium-chain triglycerides (MCT) partially rescues the testis and
169 spermatogenic defects we observed in flies (Figure S3E,S3F; one-way ANOVA with
170 Tukey multiple comparison test), as it does in mice [52,80], our data suggests flies are a
171 good model to study how *bmm*/*ATGL* influences sperm development.
172 To explore spermatogenesis in *bmm*^{1} animals, we used germline-specific marker
173 Vasa to visualize the germline in the testes of *bmm*^{1} and *bmm*^{rev} males (Figure 3D,3E)
174 [81]. We observed a significant increase in the number of germline stem cells (GSC)
175 (Figure 3F; Kruskal-Wallis rank sum test) and higher variability in GSC number in *bmm*^{1}

176 males (p=5.7×10^{-12} by F-test). Given that GSC number is affected by hub size and GSC
177 proliferation [82,83], we monitored both parameters in *bmm*^{1} and *bmm*^{rev} controls. While
178 hub size in *bmm*^{1} testes was significantly larger than in testes from *bmm*^{rev} controls
179 (Figure S3G,S3H; Welch two-sample t-test), the number of phosphohistone H3-positive
180 GSC, which indicates proliferating GSC, was unchanged in *bmm*^{1} animals (Figure S3I;
181 Kruskal-Wallis rank sum test). While this indicates a larger hub may partly explain
182 *bmm'*s effect on GSC number, *bmm* also plays a cell-autonomous role in regulating
183 GSC, as we recovered a higher proportion of *bmm*^{1} clones in the GSC pool compared
184 with *bmm*^{rev} clones at 14 days after clone induction (Figure 3G; Welch two-sample t-
185 test).

186 Beyond GSC, we uncovered additional spermatogenesis defects in *bmm*^{1} testes.
187 Peak Bam-GFP expression in testes from 0-day-old *bmm*^{1} and *bmm*^{rev} males showed
188 that GFP-positive cysts with were significantly further away from the hub in *bmm*^{1} testes
189 (Figure 3H,S3J; Welch two-sample t-test). Indeed, 15/18 *bmm*^{1} testes contained Vasa-
190 positive cysts with large nuclei in the distal half of the testis (Figure 3I, arrowheads), a
191 phenotype not present in *bmm*^{rev} testes (0/8) (p=0.0005 by Pearson's Chi-square test).
192 Because these phenotypes are also seen in testes with differentiation defects [13,84],
193 we recorded the stage of sperm development reached by the germline in *bmm*^{1} testes.
194 Most *bmm*^{1} testes contained post-meiotic cells in males raised at 25°C (Figure S3K);
195 however, germline development did not progress past the spermatocyte stage in most
196 *bmm*^{1} testes from animals raised at 29°C (Figure S3K). Testes from *bmm*^{1} males reared
197 at 25°C also had a smaller Boule-positive area (Figure 3J,S3L; Welch two-sample t-
198 test), and fewer individualization complexes and waste bags (Figure S3M,S3N; Kruskal-

199 Wallis rank sum test). Together, these data indicate loss of *bmm* delays germline
200 development. Because we recovered fewer *bmm*^{1} spermatocyte and spermatid clones
201 14 days after clone induction (Figure 3K,3L; Kruskal-Wallis rank sum test), this effect on
202 germline development represents a cell-autonomous role for *bmm*.
203

204 **_brummer_-dependent regulation of testis triglyceride levels affects**
205 **spermatogenesis**

206 *ATGL* catalyzes the first and rate-limiting step of triglyceride hydrolysis [73,85,86]. Loss
207 of this enzyme or its homologs leads to excess triglyceride accumulation
208 [27,30,67,73,75] and shifts in multiple lipid classes [66,87–89]. To determine how loss of
209 *bmm* affects spermatogenesis, we carried out mass spectrometry (MS)-based
210 untargeted lipidomic profiling of *bmm*^{1} and *bmm*^{rev} males. Hierarchical clustering of lipid
211 species suggests that *bmm*^{1} and *bmm*^{rev} males show distinct lipidomic profiles (Figure
212 4A). Overall, we detected 2464 and 1144 lipid features with high quantitative confidence
213 in positive and negative ion modes, respectively. By matching experimental *m/z*,
214 isotopic ratio, and tandem MS spectra to lipid libraries, we confirmed 293 unique lipid
215 species (Supplemental table 1). We found 107 lipids had a significant change in
216 abundance between *bmm*^{1} and *bmm*^{rev} males ($p_{adj}<0.05$): 85 species were upregulated
217 in *bmm*^{1} males and 22 lipid species were downregulated. Among differentially regulated
218 species from different lipid classes, triglyceride had the largest residual above expected
219 proportion ($p=5.00\times10^{-4}$ by Pearson's Chi-squared test). This suggests triglyceride is the
220 lipid class most affected by loss of *bmm* (Figure 4B,4C).

221 In *bmm*^{1} males, most triglyceride species (55/97) were significantly higher.
222 Because we observed a positive correlation between the fold increase in triglyceride
223 abundance with both the number of double bonds (p=7.52×10^{-8} by Kendall's rank
224 correlation test; Figure S4A) and the number of carbons (p=2.77×10^{-10} by Kendall's rank
225 correlation test; Figure S4B), our data align well with *bmm*/*ATGL's* known role in
226 regulating triglyceride levels[67,68,73] and its substrate preference of long-chain
227 polyunsaturated fatty acids[85]. While we also detected changes in species such as
228 fatty acids, acylcarnitine, and membrane lipids (Figure S4C–S4H), in line with recent
229 *Drosophila* lipidomic data[90,91], the striking accumulation of triglyceride in *bmm*^{1} males
230 suggested that excess testis triglyceride in *bmm*^{1} males may contribute to their
231 spermatogenic defects. To test this, we examined spermatogenesis in *bmm*^{1} males
232 carrying loss-of-function mutations in *midway* (*mdy*). *mdy* is the *Drosophila* homolog of
233 *diacylglycerol O-acyltransferase 1* (*DGAT1*), and whole-body loss of *mdy* reduces
234 whole-body triglyceride levels[92–94]. Importantly, testes isolated from males lacking
235 both *bmm* and *mdy* (genotype *mdy*$^{QX25/k03902}$*;bmm*^{1}) had fewer LD than testes dissected
236 from *bmm*^{1} males (Figures 4D,S4I; one-way ANOVA with Tukey multiple comparison
237 test).
238 We found that testes isolated from *mdy*$^{QX25/k03902}$*;bmm*^{1} males were significantly
239 larger and had more spermatid bundles than testes from *bmm*^{1} males (Figure 4E–G;
240 one-way ANOVA with Tukey multiple comparison test). The elevated number of GSC in
241 *bmm*^{1} male testes was similarly rescued in *mdy*$^{QX25/k03902}$*;bmm*^{1} males (Figure 4H; one-
242 way ANOVA with Tukey multiple comparison test). These data suggest that defective
243 spermatogenesis in *bmm*^{1} males can be partly attributed to excess triglyceride

244 accumulation. Notably, at least some of these defects are cell-autonomous: RNAi-
245 mediated knockdown of *mdy* in the germline of *bmm*^{1} males partially rescued the
246 defects in testis size (Figure 4I; Kruskal-Wallis rank sum test with Dunn's multiple
247 comparison test) and GSC variance (Figure S4J; p=4.5 x 10^{-5} and 8.2 x 10^{-3} by F-test
248 from the GAL4- and UAS-only crosses, respectively). *bmm*-mediated regulation of testis
249 triglyceride therefore plays a previously unrecognized role in regulating sperm
250 development.
251
252 **DISCUSSION**
253 In this study, we used *Drosophila* to gain insight into how the neutral lipids, a major lipid
254 class, contribute to sperm development. We describe the distribution of LD under
255 normal physiological conditions in the *Drosophila* testis, and show that LD are present
256 at the early stages of development in both somatic and germline cells. While many
257 factors are known to regulate LD in nongonadal cell types, we reveal a cell-autonomous
258 role for triglyceride lipase *bmm* in regulating testis LD during spermatogenesis. Indeed,
259 our data indicates loss of *bmm* delays germline differentiation leading to an
260 accumulation of early-stage germ cells. These defects in germline differentiation can be
261 partially explained by the excess accumulation of triglyceride in flies lacking *bmm*, as
262 genetically blocking triglyceride synthesis rescues multiple spermatogenic defects in
263 *bmm* mutants. Together, our data reveals previously unrecognized roles for LD and
264 triglycerides during spermatogenesis, and for *bmm* as an important regulator of testis
265 LD and germline development under normal physiological conditions.
266

267 One key outcome of our study was increased knowledge of LD regulation and
268 function in the testis. Despite rapidly expanding knowledge of LD in cell types such as
269 adipocytes or skeletal muscle, less is known about how LD influence spermatogenesis
270 under normal physiological conditions. In mammals, testis LD contain cholesterol and
271 play a role in promoting steroidogenesis [95,96]. In flies, we show that LD are present in
272 the testis, and that excess accumulation of these LD affects sperm development. In
273 nongonadal cell types, triglycerides provide a rich source of fatty acids for cellular ATP
274 production, lipid building blocks to support membrane homeostasis and growth, and
275 metabolites that can act as signaling molecules [26]. Because ATP production, lipid
276 precursors, and lipid signaling all play roles in supporting normal sperm development
277 [97,98], future studies will need to determine how each of these processes is affected
278 when excess triglyceride accumulates in testis LD. This will provide critical insight into
279 how triglyceride stored within testis LD contributes to overall cellular lipid metabolism
280 during spermatogenesis. Because of the parallel spermatogenic defects we observed in
281 *bmm* mutants and *ATGL*-deficient mice, we expect that these mechanisms will also
282 operate in other species.
283 A more comprehensive understanding of neutral lipid metabolism during sperm
284 development will also emerge from studies on the upstream signaling networks that
285 regulate testis LD and triglyceride. Given that we show an important and cell-
286 autonomous role for *bmm* in regulating testis LD and triglyceride, future studies will
287 need to identify factors that regulate *bmm* in the testis. Based on public single-cell
288 RNAseq data and the *bmm-GFP* reporter strain, our data suggest *bmm* mRNA levels
289 are differentially regulated between early and later stages of sperm development.

290 Candidates for mediating this regulation include the insulin/insulin-like growth factor
291 signaling pathway (IIS), Target of rapamycin (TOR) pathway, and nuclear factor
292 κB/Relish pathway (NFκB), as all of these pathways influence *bmm* mRNA levels in
293 nongonadal cell types [99–105]. Beyond mRNA levels, Bmm protein levels and post-
294 translational modifications may also be differentially regulating during spermatogenesis.
295 For example, studies show that the proteins encoded by *bmm* homologs in other
296 animals are regulated by phosphorylation [106], mediated by kinases such as
297 adenosine monophosphate-activated protein kinase (AMPK) and protein kinase A
298 (PKA) [107–109]. Importantly, many of these pathways, including IIS, TOR, AMPK,
299 NFκB and possibly PKA influence *Drosophila* sperm development [110–115]. Identifying
300 the signaling networks that influence *bmm* regulation during sperm development will
301 therefore lead to a deeper understanding of how testis LD and triglyceride are
302 coordinated with physiological factors to promote normal spermatogenesis. Because
303 pathways such as IIS and AMPK, and others, regulate sperm development in other
304 species [116–118], these insights may reveal conserved mechanisms that govern the
305 regulation of cellular neutral lipid metabolism during sperm development.
306
307
308

309 **ACKNOWLEDGEMENTS**

310 We thank Dr. Ronald Kühnlein for *bmm*^{1} and *bmm*^{rev} lines [67], Dr. Michael Welte for
311 *UAS-GFP-LD*[58], and Dr. Kaeko Kamei for *bmm-GFP* [77]. We used stocks from the
312 Bloomington *Drosophila* Stock Center (NIH P40OD018537) and Vienna *Drosophila*
313 Resource Center (VDRC). We acknowledge critical resources and information provided
314 by FlyBase [119] (supported by the National Human Genome Research Institute at the
315 U.S. National Institutes of Health (U41 HG000739) and the British Medical Research
316 Council (MR/N030117/1)). This work was supported by the Life Sciences Institutes
317 Imaging Core, supported by the UBC GREx Biological Resilience Initiative. Funding for
318 this study was provided by grants to EJR from the Canadian Institutes for Health
319 Research (PJT-153072), Michael Smith Foundation for Health Research (16876), and
320 the Canadian Foundation for Innovation (JELF-34879). GT was supported by a grant
321 from the Natural Sciences and Engineering Research Council (NSERC; 2018-04648),
322 TH/HY/CW were supported by NSERC (2020-04895), MA was supported by the
323 Jacob's foundation. We would like to acknowledge that our research takes place on the
324 traditional, ancestral, and unceded territory of the Musqueam people; a privilege for
325 which we are grateful.

326

327 **AUTHOR CONTRIBUTIONS**

328 Conceptualization, C.C. and E.J.R.; Methodology, C.C. and Y.Y.P.; Software, C.C.;
329 Investigation, C.C., H.Y., and Y.Y.P.; Lipidomics, M.A., H.Y., C.W., T.H.; Writing –
330 Original Draft, C.C. and E.J.R.; Writing – Review and Editing, C.C., E.J.R., and Y.Y.P.;

331 Supervision, E.J.R., G.T., and T.H.; Project administration, E.J.R.; Funding Acquisition,
332 E.J.R., G.T., and T.H.
333
334 **DECLARATION OF INTERESTS**
335 The authors declare no competing interests.
336
337 **FIGURE LEGENDS**
338 **Figure 1 – Lipid droplets are present in early-stage somatic and germ cells.** (A)
339 Testis lipid droplets (LD) in *w*^{1118} animals visualized with neutral lipid dye BODIPY.
340 (A,A') Scale bar=50 μm; (A'',A''') scale bar=15 μm. Asterisk indicates hub in all images.
341 Arrows point to LD; arrowheads point to spermatocytes in A,B. (B) Testis LD visualized
342 with BODIPY in newly-eclosed males from two wild-type genotypes. Scale bars: main
343 image=50 μm; inset image=10 μm. (C) Testis LD from *w*^{1118} animals at different times
344 post-eclosion. Scale bars=50 μm. (D) Testis LD visualized with LipidTox Red in animals
345 with somatic cell overexpression of GFP-LD (*Tj-GAL4>UAS-GFP-LD*). GFP- and
346 LipidTox Red-positive punctae are somatic LD (D–D'' arrows); LipidTox punctae without
347 GFP indicate germline LD (D–D'' arrowheads). Scale bars=10 μm. (E) Histogram
348 showing the spatial distribution of somatic cell LD; error bars represent standard error of
349 the mean (SEM). (F) Cumulative frequency distributions of somatic LD (blue line, data
350 reproduced from E), zfh-1-positive somatic cells (zfh-1^{+} cells, orange line), and Eya-
351 positive somatic cells (Eya^{+} cells, grey line). (G) Testis LD visualized with LipidTox Red
352 in males with germline overexpression of GFP-LD (*nos-GAL4>UAS-GFP-LD*). GFP- and
353 LipidTox Red-positive punctae indicate germline LD (arrows); LipidTox punctae without

354 GFP indicate non-germline LD (arrowheads). Scale bars=10 μm. (H) Histogram
355 representing the spatial distribution of LD within the germline; error bars represent SEM.
356 (I) Histogram representing the spatial distribution of LD and GFP fluorescence (green
357 line) (arbitrary units, a.u.) in a representative testis of a *bam-GFP* animal (panel J). (J)
358 Testis LD in a *bam-GFP* animal; arrows point to LD and arrowheads point to
359 spermatocytes. Scale bar=50 μm. See also Supplemental Figure 1.
360
361 **Figure 2 – *bmm* regulates testis lipid droplets in a cell-autonomous manner.** (A)
362 Testis lipid droplets (LD) indicated by LipidTox Red in *bmm-GFP* animals. Arrows point
363 to LD in all images. Arrowheads point to spermatocytes. Scale bars=50 μm. Asterisks
364 indicate the hub in all images. (B) Quantification of nuclear GFP intensity in testes
365 isolated from *bmm-GFP* animals (n=3). Germline stem cell (GSC), spermatogonia (SG),
366 spermatocyte (SC). (C) Spatial distribution of LD (grey histogram) and GFP expression
367 (green line) in testes from *bmm-GFP* animals as a function of distance from the hub
368 (n=3). (D,E) LD near the apical region of the testis in bmm^{rev} (D) or bmm^{1} (E) animals.
369 (F) LD further away from the apical tip in bmm^{1} animals. (D–F) Scale bars=50 μm. (G)
370 Histogram representing testis LD size distribution in bmm^{rev} (grey) and bmm^{1} (orange).
371 (H) Apical tip of the testes is at the left of the graph; individual dots represent a single
372 LD and its relative position to the hub marked by an asterisk. Cumulative frequency
373 distribution of the distance between LDs and the apical tip of the testes are drawn as
374 solid lines. (I) Number of testis LD in bmm^{rev} (grey) or bmm^{1} (orange) in FLP-FRT
375 clones 3 days post-clone induction; dots represent measurements from a single clone.

376 The number of cells in each cyst (CC) counted is indicated. See also Supplemental
377 Figure 2.
378
379 **Figure 3 – A cell-autonomous role for *bmm* in regulating spermatogenesis.** Testes
380 isolated from *bmm*^{rev} (A) and *bmm*^{1} (A') animals raised at 29°C stained with phalloidin.
381 Scale bars=100 µm. (B) Testis size in *bmm*^{1} and *bmm*^{rev} animals raised at 29°C. (C)
382 Spermatid bundle number in *bmm*^{1} and *bmm*^{rev} testes from animals reared at 29°C.
383 (D,E) Representative images of *bmm*^{rev} (D) or *bmm*^{1} (E) testes stained with DAPI and
384 anti-Vasa antibody. Arrows indicate germline stem cells (GSC). Scale bar=50 µm. The
385 hub is marked by an asterisk in all images. (F) GSC number in *bmm*^{1} and *bmm*^{rev}
386 testes. (G) Proportion of GSCs that were either *bmm*^{1} or *bmm*^{rev} clones at 3 and 14
387 days post-clone induction. (H) Representative images of *bmm*^{rev} (H) and *bmm*^{1} (H')
388 testes carrying *bam-GFP*; data quantified in Figure S3J. Arrows indicate regions with
389 high Bam-GFP. Scale bars=50 µm. (I) Representative images of *bmm*^{rev} (I) or *bmm*^{1}
390 (I',I'') testes stained with anti-Vasa antibody. Arrows indicate Vasa-positive cysts in
391 *bmm*^{1} testis. Panel I'' is magnified from the boxed region in I'. (I,I') Scale bars=100 µm;
392 (I'') scale bar=50 µm. (J) Maximum projection of *bmm*^{rev} (J) or *bmm*^{1} (J') testes stained
393 with anti-Boule antibody (green) and DAPI (blue). Scale bars=100 µm. Number of *bmm*^{1}
394 and *bmm*^{rev} spermatocyte clones (K) or post-meiotic clones (L) at 3 and 14 days post-
395 clone induction. See also Supplemental Figure 3.
396
397 **Figure 4 – Loss of *bmm* disrupts triglyceride homeostasis and leads to**
398 **spermatogenic defects.** (A) Hierarchical clustering of lipid species detected in *bmm*^{rev}

399 and *bmm*^{1} animals. (B) Histograms showing the proportion of species in each lipid class
400 with different levels between *bmm*^{1} and *bmm*^{rev}. Numbers on histograms indicate the
401 number of species with differences in abundance. (C) Volcano plot showing fold change
402 in abundance of triglycerides (green; 97 species) and non-triglyceride lipids (grey; 186
403 species) in our dataset. (D) Arrows indicate testis LD stained with LipidTox Red in
404 *bmm*^{rev} (D), *bmm*^{1} (D'), or *mdy*$^{QX25/k03902}$; *bmm*^{1} (D'') animals. (E) Whole testes isolated
405 from *bmm*^{rev} (E), *bmm*^{1} (E'), or *mdy*$^{QX25/k03902}$;*bmm*^{1} (E'') animals stained with anti-Vasa
406 antibody (red) and DAPI (blue). Arrowheads indicate spermatid bundles. Scale
407 bars=100 μm. (F) Testis size in *bmm*^{rev}, *bmm*^{1}, and *mdy*$^{QX25/k03902}$;*bmm*^{1} animals.
408 Spermatid bundles (G) and number of germline stem cells (H) in *bmm*^{rev}, *bmm*^{1}, and
409 *mdy*$^{QX25/k03902}$;*bmm*^{1} animals. (I) Testis size in animals with germline-specific *mdy*
410 knockdown (*nos-GAL4>mdy RNAi*; *bmm*^{1}) compared with controls (*nos-GAL4>+*; *bmm*^{1}
411 and +>*mdy RNAi*; *bmm*^{1}). See also Supplemental Figure 4.
412

413 **MATERIALS AND METHODS**

414

415 ***Materials and Resource availability.*** *Drosophila* strains and their source are listed in a
416 Key Resources table. Further information and requests for resources and reagents
417 should be directed to, and will be fulfilled by, lead contact Dr. Elizabeth J. Rideout
418 (elizabeth.rideout@ubc.ca).

419

420 ***Data and Code availability.*** All raw data and results of statistical tests reported in this
421 paper are located in Supplementary files 1-4. This paper does not report original code.
422 Any additional information required to reanalyze the data reported in this paper is
423 available from the lead contact upon request.

424

425 ***Fly husbandry.*** Fly stocks were maintained at room temperature in 12:12 hour
426 light:dark cycle. Unless otherwise indicated, all flies were raised at 25°C with a density
427 of 50 larvae per 10 mL fly media. Because this project examines sperm development,
428 we used male flies in all experiments. Fly media contained 20.5 g sucrose (SU10, Snow
429 Cap), 70.9 g Dextrose (SUG8, Snow Cap), 48.5 g cornmeal (AO18006, Snow Cap),
430 30.3 g baker's yeast (NB10, Snow Cap), 4.55 g agar (DR-820-25F, SciMart), 0.5 g
431 calcium chloride dihydrate (CCL302.1, BioShop Canada), 0.5 g magnesium sulfate
432 heptahydrate (MAG511.1, BioShop Canada), 4.9 mL propionic acids (P1386, Sigma-
433 Aldrich), and 488 µL phosphoric acid (P5811, Sigma-Aldrich) per 1L of media. For diets
434 with medium- or long-chain triglyceride, 4 g of coconut oil (medium chain triglyceride) or
435 olive oil (long chain triglyceride) was added per 100 mL of media described above prior

436 to cooling. Males were collected and dissected within 24 hours of eclosion unless
437 otherwise indicated. Fixations were performed at room temperature with 4%
438 paraformaldehyde (CA11021-168, VWR) in PBS for 20 minutes on a rotating platform
439 followed by washing in PBS twice before staining. Fly strains used in our study are
440 listed in a Key Resources table.
441
442 ***Testis cell stage classification and measurements*.** Cells at an early stage of
443 development (stem cells and early-stage somatic and germline cells) were located in
444 the apical region of the testis, and were identified by their small and dense nuclei[120].
445 GSC were defined as Vasa-positive cells in direct contact with the hub; proliferating
446 GSC were identified as Vasa-positive cells in direct contact with the hub that were also
447 phospho-H3 positive. Cells in the testis region occupied by primary spermatocytes were
448 identified by their large cell size and decondensed chromosome staining occupying
449 three nuclear domains[120]. Spermatid bundles were identified by their condensed and
450 needle-shaped nuclei, which roughly corresponds to nuclei with protamine-based
451 chromatin[121]. Testis size was measured by quantifying the length of a line drawn
452 down the middle of a testis image; starting from the apical tip of the testis and ending
453 where the testis meets the seminal vesicle.
454
455 ***FLP-FRT clone induction.*** Adult males were collected at 3-5 days post-eclosion and
456 heat-shocked three times at 37°C with a 10 min rest period at room temperature
457 between heat shocks. After heat-shock, the flies were incubated at room temperature
458 until dissection.

459

460 ***Immunohistochemistry.*** Fixed samples were rinsed three times with blocking solution
461 containing 0.2% bovine serum albumin (A4503, Sigma-Aldrich), 0.3% Triton-X in PBS,
462 then blocked for 1 hr on a rotating platform at room temperature. During the incubation,
463 the blocking solution was changed every 15 minutes. After blocking, the sample were
464 resuspended in blocking solution with the appropriate concentration of primary antibody
465 (see Key Resources table), and incubated overnight at 4°C. Samples were rinsed three
466 times with blocking solution after removing primary antibody, and blocked for one hour
467 on a rotating platform in blocking solution. Secondary antibody was applied in blocking
468 solution and left on the rotating platform at room temperature for 40 min. The sample
469 was rinsed with blocking solution three more times, and washed four times for 15 min
470 per wash in blocking solution. Testis samples were resuspended in Vectashield
471 mounting media with DAPI (H-1200-10, Vector Laboratory) or SlowFade Diamond
472 mounting media (S36972, Thermo Fisher Scientific) prior to mounting.

473

474 ***Lipid droplet staining.*** Fixed testes were briefly permeabilized with 0.1% Triton-X in
475 PBS for 5 min prior to applying phalloidin. For BODIPY staining, samples were
476 suspended in PBS containing 10 µg/mL DAPI (2879083-5mg, PeproTech), 1:500
477 BODIPY 495/503 (Thermo Fisher Scientific D3922), and 1:1000 phalloidin iFluor647
478 (ab176759, Abcam) or 1:40 phalloidin TexasRed (T7471, Thermo Fisher Scientific). For
479 staining with LipidTox Red, samples were suspended in PBS containing 10 µg/mL DAPI
480 (2879083-5mg, PeproTech), 1:200 LipidTox Red (H34476, Thermo Fisher Scientific),
481 and 1:1000 phalloidin iFluor647 (ab176759, Abcam). For staining free sterols, samples

482 were prepared as for BODIPY staining with 50 µg/mL filipin in place of BODIPY for 30
483 min. Samples were incubated on a rotating platform for 40 minutes at room
484 temperature. After incubation, samples were washed twice with PBS, then resuspended
485 in SlowFade Diamond mounting media (Thermo Fisher Scientific S36972) prior to
486 mounting.
487
488 ***Image acquisition and processing.*** All images were acquired on a Leica SP5 confocal
489 microscope system with 20X or 40X objectives and quantified with Fiji image analysis
490 software[122].
491
492 ***Drosophila lipidomics.*** *Drosophila* extracts were prepared following the previously
493 reported protocol[123]. Briefly, 10 *Drosophila* males (~10 mg) were weighed, 300 µL of
494 ice-cold methanol/water mixture (9:1, v:v) was added to these males, and the samples
495 were homogenized with glass beads using a bead beater (mini-beadbeater-16,
496 BioSpec, Bartlesville, Ok, USA). Sample weight was used for sample normalization. Fly
497 lysate was kept at -20°C for 4 hours for protein precipitation. Then, 900 µL of methyl
498 tert-butyl ether was added and the solution was shaken for 5 min to extract lipids. To
499 induce phase separation 285 µL of water was added, followed by centrifugation. The
500 upper layer was separated, dried, and reconstituted in isopropanol/acetonitrile (1:1, v:v)
501 for liquid chromatography-mass spectrometry (LC-MS) analysis. The volume of
502 reconstitution solution was proportional to sample weight for normalization. Quality
503 control (QC) samples were prepared by pooling 20 µL aliquot from each sample. The

504 method blank sample was prepared using an identical workflow but without adding
505 *Drosophila*.
506 *Drosophila* extracts were analyzed on an UHR-QqTOF (Ultra-High Resolution
507 Qq-Time-Of-Flight) mass spectrometry Impact II (Bruker Daltonics, Bremen, Germany)
508 interfaced with an Agilent 1290 Infinity II LC Systems (Agilent Technologies, Santa
509 Clara, CA, USA). LC separation was performed using a Waters reversed-phase (RP)
510 UPLC Acquity BEH C18 Column (1.7 μm, 1.0 mm ×100 mm, 130 Å) (Milford, MA, USA)
511 maintained at 30°C. For positive ion mode, the mobile phase A was 60% acetonitrile in
512 water and the mobile phase B was 90% isopropanol in acetonitrile, both containing 5
513 mM ammonium formate (pH = 4.8, adjusted by formic acid). For negative ion mode, the
514 mobile phase A was 60% acetonitrile in water and the mobile phase B was 90%
515 isopropanol in acetonitrile, both containing 5 mM NH_4FA (pH = 9.8, adjusted by
516 ammonium hydroxide). The LC gradient for positive and negative ion modes was set as
517 follows: 0 min, 5% B; 8 min, 40% B; 14 min, 70% B; 20 min, 95% B; 23 min, 95% B; 24
518 min, 5% B; 33 min, 5% B. The flow rate was 0.1 mL/min. The injection volume was
519 optimized to 2 μL in positive mode and 5 μL in negative mode using QC sample. The
520 ESI source conditions were set as follows: dry gas temperature, 220 °C; dry gas flow, 7
521 L/min; nebulizer gas pressure, 1.6 bar; capillary voltage, 4500 V for positive mode and
522 3000 V for negative mode. The MS1 analysis was conducted using following
523 parameters: mass range, 70-1000 m/z; spectrum type: centroid, calculated using
524 maximum intensity; absolute intensity threshold: 250. Data-dependent MS/MS analysis
525 parameters: collision energy: 16-30 eV; cycle time, 3 s; spectra rate: 4 Hz when
526 intensity < 10^4 and 12 Hz when intensity > 10^5, linearly increased from 10^4 to 10^5.

527 External calibration was applied using sodium formate to ensure the m/z accuracy
528 before sample analysis.
529 The raw LC-MS data were processed using MS-DIAL (ver. 4.38)[124]. The
530 detailed MS-DIAL parameters are: MS1 tolerance, 0.01 Da; MS/MS tolerance, 0.05;
531 mass slice width, 0.05 Da; smoothing method, linear weighted moving average;
532 smoothing level, 3 scans; minimum peak width, 5 scans. Lipid features with high
533 quantitative confidence were selected by the following criteria: retention time was within
534 the gradient elution time (< 23 min); average intensity in QC samples is larger than 5-
535 fold of the intensity in method blank sample. Lipid identification was performed by
536 matching experimental precursor m/z, isotopic ratio and MS/MS spectrum against the
537 LipidBlast libraries embedded in MS-DIAL. To improve the quantification accuracy, the
538 measured MS signal intensities were corrected using serial diluted QC samples
539 following the reported workflow[125].
540
541 **Quantification and statistical analysis.** All microscopy images were quantified using
542 Fiji software[122]. For lipid droplet counts, a single optical slice through the middle of
543 the testis containing the hub was used with the exception of FLP-FRT experiment where
544 all lipid droplets within a GFP-negative cyst were counted (Figure 2I). All statistical
545 analyses were done using R (obtained from https://cran.r-project.org). With exception of
546 data concerning spatial distribution, and lipidomic data, Shapiro-Wilk test (via
547 *shapiro.test* in base R) was used to assess normality of distribution prior to testing for
548 significance. Kruskal-Wallis rank sum test (from the R package *coin*) and Dunn's test
549 (from the R package *dunn.test*) were used in place of Welch two-sample t-test and

550 Tukey's multiple comparison test when the assumption of normality was not met. For
551 testing differences in variance between two populations, F-test (via *var.test* in base R)
552 was used. For testing differences in spatial distribution, two-sample Kolmogorov-
553 Smirnov test (via *ks.test* in base R) was used. All *p*-values are indicated in figures;
554 extremely small *p*-values are listed as $p<2.2 \times 10^{-16}$.
555

556 **RESOURCE TABLE**

REAGENT or RESOURCE	SOURCE	RESOURCE #
Antibodies		
Anti-Vasa (1:200)	Gift from Dr. R. Lehman, MIT	
Anti-Eya (1:50)	Developmental Studies Hybridoma Bank (DSHB)	eya10H6
Anti-zfh1 (1:1000)	Gift from Dr. J. Skeath, WUSTL	
Anti-boule (1:1000)	Gift from Dr. S. Wasserman, UCSD	
Anti-phospho-histone H3 (1:1000)	Millipore Sigma	05-1354
Experimental models: *Drosophila melanogaster*		
w^{1118}	Bloomington *Drosophila* stock center	3605
CantonS	Bloomington *Drosophila* stock center	64349
OregonR	Bloomington *Drosophila* stock center	25211
bmm^{1}	Gift from Dr. R. Kühnlein	
bmm^{rev}	Gift from Dr. R. Kühnlein	
mdy[Qx25], cn[1], bw[1]/CyO, l(2)DTS513[1]	Bloomington *Drosophila* stock center	5095
y[1],w[67c23];P{lacW}Cse1[k03802],mdy[k03902]/CyO	Bloomington *Drosophila* stock center	10536
w[1118];P{GD1749}v6367 (UAS-mdy-RNAi)	Vienna *Drosophila* resource center	6367

REAGENT or RESOURCE	SOURCE	RESOURCE #
nos-GAL4::VP16	Bloomington *Drosophila* stock center	7303
Tj-GAL4	Gift from Dr. D. Godt, University of Toronto	
c587-GAL4	Bloomington *Drosophila* stock center	67747
Bam-GFP	[40]	
bmm-GFP	Gift from Dr. K. Kamei[57]	
GFP-LD	Gift from Dr. M. Welte[36]	
P{neoFRT}82B, bmm[1]	This study	
P{neoFRT}82B, bmm[rev]	This study	
bam-GFP, bmm[1]	This study	
bam-GFP, bmm[rev]	This study	
Software and algorithms		
Fiji	https://imagej.net/software/fiji/	
R	https://cran.r-project.org	

557

558 **SUPPLEMENTAL TABLE AND FILES**

559 **Supplemental table 1** – Table showing identified lipid species from untargeted

560 lipidomic analysis.

561 **Supplementary file 1** – Raw data and statistical outputs from Figure 1.

562 **Supplementary file 2** – Raw data and statistical outputs from Figure 2 and

563 Supplemental figure 2.

564 **Supplementary file 3** – Raw data and statistical outputs from Figure 3 and
565 Supplemental figure 3.
566 **Supplementary file 4** – Raw data and statistical outputs from Figure 4 and
567 Supplemental figure 4.
568
569 **SUPPLEMENTAL FIGURE LEGENDS**
570 **Supplemental Figure 1 related to Figure 1 – Cholesterol is absent from testis lipid**
571 **droplets.** (A) Testes stained with BODIPY (A) to detect neutral lipids and Filipin III (A')
572 to detect free cholesterol. Scale bars=50 μm.
573
574 **Supplemental Figure 2 related to Figure 2 – *bmm* mRNA levels during**
575 **spermatogenesis in germline and somatic lineages.** (A) Pseudotime trajectory of
576 germline (black line) based on single-cell RNA sequencing data[62]. Individual cells are
577 labeled according to the annotation within the data set. (B) Rolling average of
578 normalized *bmm* transcript counts in the germline along the trajectory shown in panel A
579 are plotted as a black line on the upper panel. Composition of cell types mapped on to
580 the trajectory at each time point is shown at the lower half of panel B. (C) Pseudotime
581 trajectory of the somatic cells (black line) based on publicly available single-cell RNA
582 sequencing data[62]. Individual cells are labeled according to the annotation within the
583 data set. (D) Rolling average of normalized *bmm* transcript counts in somatic cells
584 plotted as a black line along the trajectory shown in C (upper panel). Composition of cell
585 types mapped on to the trajectory at each time point (lower panel). (E-H)
586 Representative images of bmm^{rev} (E and F) and bmm^{1} (G and H) testes with somatic

587 over-expression of *GFP-LD* (*Tj-GAL4>UAS-GFP-LD*). Panel F and H contain magnified
588 images of the area indicated by the boxes in panel E and G, respectively. In *bmm*^{rev}
589 testes, LD were restricted to a region near the apical tip (E) of the testis in both somatic
590 (F–F''' arrows) and germline cells (F–F''' arrowheads). In *bmm*^{1} testes, LD were present
591 in both somatic (G–H arrows) and germline cells (G–H arrowheads), near the apical tip
592 of the testis in a region corresponding to early-stage germ cells and in the region
593 corresponding to spermatocytes. (E,G) Scale bars=50 μm; (F,H) scale bars=20 μm.
594
595 **Supplemental Figure 3 related to Figure 3 – Additional characterization of testis**
596 **development and spermatogenesis in animals lacking *bmm*.** (A) Testis size was
597 smaller in *bmm*^{1} mutant animals compared with *bmm*^{rev} controls at <24 hr post-eclosion
598 when raised at 25°C (A; Welch two-sample t-test). (B) The number of spermatid bundles
599 was significantly lower in *bmm*^{1} mutant animals compared with *bmm*^{rev} controls at <24
600 hr post-eclosion when raised at 25°C (Kruskal-Wallis rank sum test). (C) Testis size was
601 significantly smaller in *bmm*^{1} mutant males compared with *bmm*^{rev} control males at 14-
602 days post-eclosion (Welch two-sample t-test). (D) While the median number of
603 spermatid bundles was not significantly different between *bmm*^{1} mutant males and
604 *bmm*^{rev} control males at 14 days post-eclosion (Welch two-sample t-test), 8/27 *bmm*^{1}
605 testis had no spermatid bundles, a phenotype absent in age-matched *bmm*^{rev} males
606 (0/22) (p=0.0163, Pearson's Chi-squared test), suggesting a subtle defect is present.
607 (E) Food supplemented with 4% medium chain triglyceride (MCT), but not long chain
608 triglyceride (LCT), significantly increased testis length in *bmm*^{1} animals but had no effect
609 on this phenotype in *bmm*^{rev} control animals (one-way ANOVA with Tukey multiple

610 comparison test). (F) Food supplemented with 4% medium chain triglyceride
611 significantly increased the number of spermatid bundles in *bmm*^{1} testes but had no
612 effect on this phenotype in *bmm*^{rev} control animals (one-way ANOVA with Tukey
613 multiple comparison test). (G) Representative images of *bmm*^{rev} (G–G') or *bmm*^{1} (G''–
614 G''') testes stained for Fas3 (G and G'') and Vas (G' and G'''). Scale bars=25 μm. (H)
615 Quantification of hub area in *bmm*^{rev} or *bmm*^{1} testes showed a significantly larger hub
616 size in *bmm*^{1} testes (Welch two-sample t-test). (I) The number of germline stem cells
617 (GSC) undergoing mitosis (phospho-histone H3^{+} GSC/total GSC) was not significantly
618 different between *bmm*^{1} and *bmm*^{rev} testes (Kruskal-Wallis rank sum test). (J) The
619 distance between the hub and the first Bam-GFP positive cyst (Figure 3H) was
620 significantly higher in *bmm*^{1} testes than in *bmm*^{rev} testes (Welch two-sample t-test). (K)
621 All *bmm*^{rev} testes and most *bmm*^{1} testes contained spermatids when raised at 25°C;
622 however, the most advanced stage of spermatogenesis observed in the majority of
623 *bmm*^{1} testes isolated from animals reared at 29°C was the spermatocyte stage. (L)
624 Testes isolated from *bmm*^{1} animals showed a significantly smaller Boule-positive area
625 than control testes (Welch two-sample t-test). (M) Testes isolated from *bmm*^{1} animals
626 contain fewer individualization complexes than *bmm*^{rev} control testes (Kruskal-Wallis
627 rank sum test). (N) Fewer waste bags were present in testes isolated from *bmm*^{1}
628 animals compared with *bmm*^{rev} control testes (Kruskal-Wallis rank sum test).
629
630 **Supplemental Figure 4 related to Figure 4 – Lipidomic analysis of animals lacking**
631 ***bmm*.** (A) Higher fold-changes of triglycerides in *bmm*^{1} animals were associated with
632 less saturation in the acyl-groups (Kendall's rank correlation test). (B) Higher fold-

633 changes of triglycerides in *bmm*^{1} animals were associated with higher number of
634 carbons in the acyl-groups (Kendall's rank correlation test). Each dot represents a single
635 triglyceride species for panel B and C. (C) Volcano plot of identified lipids;
636 monoglycerides shown in blue and diglycerides shown in orange. Many monoglycerides
637 and diglycerides show increase in fold-change in *bmm*^{1} males. (D) The number of
638 carbon and the degree of saturation of monoglycerides (MAG) and diglycerides (DAG)
639 with significant changes in abundance between *bmm*^{1} and *bmm*^{rev} males. (E) Volcano
640 plot of identified lipids; fatty acids shown in magenta and acyl-carnitine shown in green.
641 Many fatty acids show an increase in fold-change while many acyl-carnitines show a
642 decrease in fold-change in *bmm*^{1} males. (F) The number of carbon and the degree of
643 saturation of fatty acids (FA) and acyl-carnitines (ACar) with significant changes in
644 abundance between *bmm*^{1} and *bmm*^{rev} males. (G) Volcano plot of identified lipids;
645 membrane lipids shown in yellow. (H) The number of carbon and the degree of
646 saturation of membrane lipids with significant changes in abundance between *bmm*^{1}
647 and *bmm*^{rev} males. For panel G and H, PC: phosphatidylcholine; PE:
648 phosphatidylethanolamine; PI: phosphatidylinositol; LPC: lysophosphatidylcholine; LPE:
649 lysophosphatidylethanolamine; SM: sphingomyelin; PG: phosphatidylglycerol. (I) Loss
650 of *mdy* function rescued the elevated number of LD in *bmm*^{1} testes to control levels
651 (one-way ANOVA with Tukey multiple comparison test). (J) Germline-specific loss of
652 *mdy* in *bmm*^{1} animals did not reduce GSC numbers, but the variance in GSC number
653 was significantly rescued (*nos-GAL4*>+; *bmm*^{1} vs *nos-GAL4*>*mdy RNAi*; *bmm*^{1}: p=4.5 ×
654 10^{-5}; +>*mdy RNAi*; *bmm*^{1} vs *nos-GAL4*>*mdy RNAi*; *bmm*^{1}: p=0.0082 by F-test).
655
656

657 **REFERENCES**
658

659 1. Brill JA, Yildirim S, Fabian L. Phosphoinositide signaling in sperm development.
660 Semin Cell Dev Biol. 2016;59: 2–9. doi:10.1016/j.semcdb.2016.06.010

661 2. Keber R, Rozman D, Horvat S. Sterols in spermatogenesis and sperm maturation. J
662 Lipid Res. 2013;54: 20–33. doi:10.1194/jlr.R032326

663 3. Rato L, Alves MG, Socorro S, Duarte AI, Cavaco JE, Oliveira PF. Metabolic
664 regulation is important for spermatogenesis. Nat Rev Urol. 2012;9: 330–338.
665 doi:10.1038/nrurol.2012.77

666 4. Wang C, Huang X. Lipid metabolism and Drosophila sperm development. Sci China
667 Life Sci. 2012;55: 35–40. doi:10.1007/s11427-012-4274-2

668 5. de Cuevas M, Matunis EL. The stem cell niche: lessons from the Drosophila testis.
669 Dev Camb Engl. 2011;138: 2861–2869. doi:10.1242/dev.056242

670 6. Demarco RS, Eikenes ÅH, Haglund K, Jones DL. Investigating Spermatogenesis in
671 Drosophila melanogaster. Methods San Diego Calif. 2014;68: 218–227.
672 doi:10.1016/j.ymeth.2014.04.020

673 7. Fabian L, Brill JA. Drosophila spermiogenesis: Big things come from little packages.
674 Spermatogenesis. 2012;2: 197–212. doi:10.4161/spmg.21798

675 8. Brill JA, Hime GR, Scharer-Schuksz M, Fuller MT. A phospholipid kinase regulates
676 actin organization and intercellular bridge formation during germline cytokinesis.
677 Development. 2000;127: 3855.

678 9. Giansanti MG, Bonaccorsi S, Kurek R, Farkas RM, Dimitri P, Fuller MT, et al. The
679 Class I PITP Giotto Is Required for Drosophila Cytokinesis. Curr Biol. 2006;16:
680 195–201. doi:10.1016/j.cub.2005.12.011

681 10. Wong R, Hadjiyanni I, Wei H-C, Polevoy G, McBride R, Sem K-P, et al. PIP2
682 Hydrolysis and Calcium Release Are Required for Cytokinesis in Drosophila
683 Spermatocytes. Curr Biol. 2005;15: 1401–1406. doi:10.1016/j.cub.2005.06.060

684 11. Wong R, Fabian L, Forer A, Brill JA. Phospholipase C and myosin light chain
685 kinase inhibition define a common step in actin regulation during cytokinesis. BMC
686 Cell Biol. 2007;8: 15. doi:10.1186/1471-2121-8-15

687 12. Amoyel M, Hillion K-H, Margolis SR, Bach EA. Somatic stem cell differentiation is
688 regulated by PI3K/Tor signaling in response to local cues. Dev Camb Engl.
689 2016;143: 3914. doi:10.1242/dev.139782

690 13. Fairchild MJ, Islam F, Tanentzapf G. Identification of genetic networks that act in
691 the somatic cells of the testis to mediate the developmental program of

692 spermatogenesis. PLOS Genet. 2017;13: e1007026.
693 doi:10.1371/journal.pgen.1007026

694 14. Inaba M, Venkei ZG, Yamashita YM. The polarity protein Baz forms a platform for
695 the centrosome orientation during asymmetric stem cell division in the Drosophila
696 male germline. eLife. 2015;4: e04960. doi:10.7554/eLife.04960

697 15. Krahn MP, Klopfenstein DR, Fischer N, Wodarz A. Membrane Targeting of
698 Bazooka/PAR-3 Is Mediated by Direct Binding to Phosphoinositide Lipids. Curr
699 Biol. 2010;20: 636–642. doi:10.1016/j.cub.2010.01.065

700 16. Papagiannouli F, Berry CW, Fuller MT. The Dlg Module and Clathrin-Mediated
701 Endocytosis Regulate EGFR Signaling and Cyst Cell-Germline Coordination in
702 the Drosophila Testis. Stem Cell Rep. 2019;12: 1024–1040.
703 doi:10.1016/j.stemcr.2019.03.008

704 17. Ueishi S, Shimizu H, Inoue YH. Male Germline Stem Cell Division and
705 Spermatocyte Growth Require Insulin Signaling in Drosophila. Cell Struct Funct.
706 2009;34: 61–69. doi:10.1247/csf.08042

707 18. Phan VH, Herr DR, Panton D, Fyrst H, Saba JD, Harris GL. Disruption of
708 Sphingolipid Metabolism Elicits Apoptosis-Associated Reproductive Defects in
709 Drosophila. Dev Biol. 2007;309: 329–341. doi:10.1016/j.ydbio.2007.07.021

710 19. Steinhauer J, Gijón MA, Riekhof WR, Voelker DR, Murphy RC, Treisman JE.
711 Drosophila Lysophospholipid Acyltransferases Are Specifically Required for Germ
712 Cell Development. Mol Biol Cell. 2009;20: 5224–5235. doi:10.1091/mbc.e09-05-
713 0382

714 20. Szafer-Glusman E, Giansanti MG, Nishihama R, Bolival B, Pringle J, Gatti M, et al.
715 A Role for Very-Long-Chain Fatty Acids in Furrow Ingression during Cytokinesis in
716 Drosophila Spermatocytes. Curr Biol. 2008;18: 1426–1431.
717 doi:10.1016/j.cub.2008.08.061

718 21. Ben-David G, Miller E, Steinhauer J. Drosophila spermatid individualization is
719 sensitive to temperature and fatty acid metabolism. Spermatogenesis. 2015;5.
720 doi:10.1080/21565562.2015.1006089

721 22. Jung A, Hollmann M, Schafer MA. The fatty acid elongase NOA is necessary for
722 viability and has a somatic role in Drosophila sperm development. J Cell Sci.
723 2007;120: 2924–2934. doi:10.1242/jcs.006551

724 23. Rabionet M, Bayerle A, Jennemann R, Heid H, Fuchser J, Marsching C, et al. Male
725 meiotic cytokinesis requires ceramide synthase 3-dependent sphingolipids with
726 unique membrane anchors. Hum Mol Genet. 2015;24: 4792–4808.
727 doi:10.1093/hmg/ddv204

728 24. Santiago Valtierra FX, Peñalva DA, Luquez JM, Furland NE, Vásquez C, Reyes
729 JG, et al. Elovl4 and Fa2h expression during rat spermatogenesis: a link to the
730 very-long-chain PUFAs typical of germ cell sphingolipids. J Lipid Res. 2018;59:
731 1175–1189. doi:10.1194/jlr.M081885

732 25. Zadravec D, Tvrdik P, Guillou H, Haslam R, Kobayashi T, Napier JA, et al. ELOVL2
733 controls the level of n-6 28:5 and 30:5 fatty acids in testis, a prerequisite for male
734 fertility and sperm maturation in mice. J Lipid Res. 2011;52: 245–255.
735 doi:10.1194/jlr.M011346

736 26. Walther TC, Farese RV. Lipid Droplets and Cellular Lipid Metabolism. Annu Rev
737 Biochem. 2012;81: 687–714. doi:10.1146/annurev-biochem-061009-102430

738 27. Wat LW, Chao C, Bartlett R, Buchanan JL, Millington JW, Chih HJ, et al. A role for
739 triglyceride lipase brummer in the regulation of sex differences in Drosophila fat
740 storage and breakdown. Hassan BA, editor. PLOS Biol. 2020;18: e3000595.
741 doi:10.1371/journal.pbio.3000595

742 28. Thiele C, Spandl J. Cell biology of lipid droplets. Curr Opin Cell Biol. 2008;20: 378–
743 385. doi:10.1016/j.ceb.2008.05.009

744 29. Bosma M. Lipid droplet dynamics in skeletal muscle. Exp Cell Res. 2016;340: 180–
745 186. doi:10.1016/j.yexcr.2015.10.023

746 30. Grönke S, Müller G, Hirsch J, Fellert S, Andreou A, Haase T, et al. Dual Lipolytic
747 Control of Body Fat Storage and Mobilization in Drosophila. PLOS Biol. 2007;5:
748 e137. doi:10.1371/journal.pbio.0050137

749 31. Rambold AS, Cohen S, Lippincott-Schwartz J. Fatty Acid Trafficking in Starved
750 Cells: Regulation by Lipid Droplet Lipolysis, Autophagy, and Mitochondrial Fusion
751 Dynamics. Dev Cell. 2015;32: 678–692. doi:10.1016/j.devcel.2015.01.029

752 32. Dichlberger A, Schlager S, Maaninka K, Schneider WJ, Kovanen PT. Adipose
753 triglyceride lipase regulates eicosanoid production in activated human mast cells.
754 J Lipid Res. 2014;55: 2471–2478. doi:10.1194/jlr.M048553

755 33. Mitsche MA, Hobbs HH, Cohen JC. Patatin-like phospholipase domain–containing
756 protein 3 promotes transfers of essential fatty acids from triglycerides to
757 phospholipids in hepatic lipid droplets. J Biol Chem. 2018;293: 6958–6968.
758 doi:10.1074/jbc.RA118.002333

759 34. Rajakumari S, Rajasekharan R, Daum G. Triacylglycerol lipolysis is linked to
760 sphingolipid and phospholipid metabolism of the yeast Saccharomyces
761 cerevisiae☆. Biochim Biophys Acta BBA - Mol Cell Biol Lipids. 2010;1801: 1314–
762 1322. doi:10.1016/j.bbalip.2010.08.004

763 35. Schlager S, Goeritzer M, Jandl K, Frei R, Vujic N, Kolb D, et al. Adipose triglyceride
764 lipase acts on neutrophil lipid droplets to regulate substrate availability for lipid

765 mediator synthesis. J Leukoc Biol. 2015;98: 837–850. doi:10.1189/jlb.3A0515-
766 206R

767 36. Zanghellini J, Natter K, Jungreuthmayer C, Thalhammer A, Kurat CF, Gogg-
768 Fassolter G, et al. Quantitative modeling of triacylglycerol homeostasis in yeast -
769 metabolic requirement for lipolysis to promote membrane lipid synthesis and
770 cellular growth: Triacylglycerol mobilization in yeast. FEBS J. 2008;275: 5552–
771 5563. doi:10.1111/j.1742-4658.2008.06681.x

772 37. Bailey AP, Koster G, Guillermier C, Hirst EMA, MacRae JI, Lechene CP, et al.
773 Antioxidant Role for Lipid Droplets in a Stem Cell Niche of Drosophila. Cell.
774 2015;163: 340–353. doi:10.1016/j.cell.2015.09.020

775 38. Liu L, MacKenzie KR, Putluri N, Maletić-Savatić M, Bellen HJ. The Glia-Neuron
776 Lactate Shuttle and Elevated ROS Promote Lipid Synthesis in Neurons and Lipid
777 Droplet Accumulation in Glia via APOE/D. Cell Metab. 2017;26: 719-737.e6.
778 doi:10.1016/j.cmet.2017.08.024

779 39. Nguyen TB, Louie SM, Daniele JR, Tran Q, Dillin A, Zoncu R, et al. DGAT1-
780 Dependent Lipid Droplet Biogenesis Protects Mitochondrial Function during
781 Starvation-Induced Autophagy. Dev Cell. 2017;42: 9-21.e5.
782 doi:10.1016/j.devcel.2017.06.003

783 40. Henne M. And three's a party: lysosomes, lipid droplets, and the ER in lipid
784 trafficking and cell homeostasis. Curr Opin Cell Biol. 2019;59: 40–49.
785 doi:10.1016/j.ceb.2019.02.011

786 41. Welte MA. Expanding Roles for Lipid Droplets. Curr Biol. 2015;25: R470–R481.
787 doi:10.1016/j.cub.2015.04.004

788 42. Casado ME, Pastor O, Mariscal P, Canfrán-Duque A, Martínez-Botas J, Kraemer
789 FB, et al. Hormone-sensitive lipase deficiency disturbs the fatty acid composition
790 of mouse testis. Prostaglandins Leukot Essent Fatty Acids. 2013;88: 227–233.
791 doi:10.1016/j.plefa.2012.12.005

792 43. El-Shehawi AM, El-Shazly S, Ahmed M, Alkafafy M, Sayed S, Farouk S, et al.
793 Transcriptome Analysis of Testis from HFD-Induced Obese Rats (Rattus
794 norvigicus) Indicated Predisposition for Male Infertility. Int J Mol Sci. 2020;21:
795 6493. doi:10.3390/ijms21186493

796 44. Wang W, Wei S, Li L, Su X, Du C, Li F, et al. Proteomic analysis of murine testes
797 lipid droplets. Sci Rep. 2015;5: 12070. doi:10.1038/srep12070

798 45. Bajpai M, Gupta G, Setty BS. Changes in carbohydrate metabolism of testicular
799 germ cells during meiosis in the rat. Eur J Endocrinol. 1998;138: 322–327.

800 46. Kerr JB, Kretser DMD. CYCLIC VARIATIONS IN SERTOLI CELL LIPID CONTENT
801 THROUGHOUT THE SPERMATOGENIC CYCLE IN THE RAT. Reproduction.
802 1975;43: 1–8. doi:10.1530/jrf.0.0430001

803 47. Mori H, Christensen AK. Morphometric analysis of Leydig cells in the normal rat
804 testis. J Cell Biol. 1980;84: 340–354. doi:10.1083/jcb.84.2.340

805 48. Paniagua R, Rodríguez MC, Nistal M, Fraile B, Amat P. Changes in the lipid
806 inclusion/Sertoli cell cytoplasm area ratio during the cycle of the human
807 seminiferous epithelium. Reproduction. 1987;80: 335–341.
808 doi:10.1530/jrf.0.0800335

809 49. Demarco RS, Uyemura BS, D'Alterio C, Jones DL. Mitochondrial fusion regulates
810 lipid homeostasis and stem cell maintenance in the Drosophila testis. Nat Cell
811 Biol. 2019;21: 710–720. doi:10.1038/s41556-019-0332-3

812 50. Chen M, Wang H, Li X, Li N, Xu G, Meng Q. PLIN1 deficiency affects testicular
813 gene expression at the meiotic stage in the first wave of spermatogenesis. Gene.
814 2014;543: 212–219. doi:10.1016/j.gene.2014.04.021

815 51. Hermo L, Chung S, Gregory M, Smith CE, Wang SP, El-Alfy M, et al. Alterations in
816 the testis of hormone sensitive lipase-deficient mice is associated with decreased
817 sperm counts, sperm motility, and fertility. Mol Reprod Dev. 2008;75: 565–577.
818 doi:10.1002/mrd.20800

819 52. Masaki H, Kim N, Nakamura H, Kumasawa K, Kamata E, Hirano K, et al. Long-
820 chain fatty acid triglyceride (TG) metabolism disorder impairs male fertility: a study
821 using adipose triglyceride lipase deficient mice. MHR Basic Sci Reprod Med.
822 2017;23: 452–460. doi:10.1093/molehr/gax031

823 53. Freeman DA, Ascoli M. Studies on the source of cholesterol used for steroid
824 biosynthesis in cultured Leydig tumor cells. J Biol Chem. 1982;257: 14231–14238.

825 54. Wang F, Chen Z, Ren X, Tian Y, Wang F, Liu C, et al. Hormone-sensitive lipase
826 deficiency alters gene expression and cholesterol content of mouse testis.
827 Reproduction. 2017;153: 175–185. doi:10.1530/REP-16-0484

828 55. de Cuevas M, Matunis EL. The stem cell niche: lessons from the Drosophila testis.
829 Development. 2011;138: 2861–2869. doi:10.1242/dev.056242

830 56. Walther TC, Chung J, Jr RVF. Lipid Droplet Biogenesis. Annu Rev Cell Dev Biol.
831 2017;33: 491–510. doi:10.1146/annurev-cellbio-100616-060608

832 57. Boyle M, DiNardo S. Specification, migration and assembly of the somatic cells of
833 the Drosophila gonad. Development. 1995;121: 1815–1825.
834 doi:10.1242/dev.121.6.1815

835 58. Yu YV, Li Z, Rizzo NP, Einstein J, Welte MA. Targeting the motor regulator Klar to
836 lipid droplets. BMC Cell Biol. 2011;12: 9. doi:10.1186/1471-2121-12-9

837 59. Leatherman JL, DiNardo S. Zfh-1 Controls Somatic Stem Cell Self-Renewal in the
838 Drosophila Testis and Nonautonomously Influences Germline Stem Cell Self-
839 Renewal. Cell Stem Cell. 2008;3: 44–54. doi:10.1016/j.stem.2008.05.001

840 60. Fabrizio JJ, Boyle M, DiNardo S. A somatic role for eyes absent (eya) and sine
841 oculis (so) in drosophila spermatocyte development. Dev Biol. 2003;258: 117–
842 128. doi:10.1016/S0012-1606(03)00127-1

843 61. Chen D, McKearin DM. A discrete transcriptional silencer in the bam gene
844 determines asymmetric division of the Drosophila germline stem cell.
845 Development. 2003;130: 1159–1170. doi:10.1242/dev.00325

846 62. Insco ML, Leon A, Tam CH, McKearin DM, Fuller MT. Accumulation of a
847 differentiation regulator specifies transit amplifying division number in an adult
848 stem cell lineage. Proc Natl Acad Sci U S A. 2009;106: 22311–22316.
849 doi:10.1073/pnas.0912454106

850 63. Chen D, Wu C, Zhao S, Geng Q, Gao Y, Li X, et al. Three RNA Binding Proteins
851 Form a Complex to Promote Differentiation of Germline Stem Cell Lineage in
852 Drosophila. PLoS Genet. 2014;10. doi:10.1371/journal.pgen.1004797

853 64. Gonczy P, Matunis E, DiNardo S. bag-of-marbles and benign gonial cell neoplasm
854 act in the germline to restrict proliferation during Drosophila spermatogenesis.
855 Development. 1997;124: 4361–4371.

856 65. Athenstaedt K, Daum G. YMR313c/TGL3 Encodes a Novel Triacylglycerol Lipase
857 Located in Lipid Particles of Saccharomyces cerevisiae*. J Biol Chem. 2003;278:
858 23317–23323. doi:10.1074/jbc.M302577200

859 66. Chitraju C, Trötzmüller M, Hartler J, Wolinski H, Thallinger GG, Haemmerle G, et
860 al. The impact of genetic stress by ATGL deficiency on the lipidome of lipid
861 droplets from murine hepatocytes. J Lipid Res. 2013;54: 2185–2194.
862 doi:10.1194/jlr.M037952

863 67. Grönke S, Mildner A, Fellert S, Tennagels N, Petry S, Müller G, et al. Brummer
864 lipase is an evolutionary conserved fat storage regulator in Drosophila. Cell
865 Metab. 2005;1: 323–330. doi:10.1016/j.cmet.2005.04.003

866 68. Haemmerle G, Lass A, Zimmermann R, Gorkiewicz G, Meyer C, Rozman J, et al.
867 Defective Lipolysis and Altered Energy Metabolism in Mice Lacking Adipose
868 Triglyceride Lipase. Science. 2006;312: 734–737. doi:10.1126/science.1123965

869 69. Haemmerle G, Moustafa T, Woelkart G, Büttner S, Schmidt A, van de Weijer T, et
870 al. ATGL-mediated fat catabolism regulates cardiac mitochondrial function via
871 PPAR-α and PGC-1. Nat Med. 2011;17: 1076–1085. doi:10.1038/nm.2439

872 70. Huijsman E, van de Par C, Economou C, van der Poel C, Lynch GS, Schoiswohl G,
873 et al. Adipose triacylglycerol lipase deletion alters whole body energy metabolism
874 and impairs exercise performance in mice. Am J Physiol-Endocrinol Metab.
875 2009;297: E505–E513. doi:10.1152/ajpendo.00190.2009

876 71. Korbelius M, Vujic N, Sachdev V, Obrowsky S, Rainer S, Gottschalk B, et al.
877 ATGL/CGI-58-Dependent Hydrolysis of a Lipid Storage Pool in Murine
878 Enterocytes. Cell Rep. 2019;28: 1923-1934.e4. doi:10.1016/j.celrep.2019.07.030

879 72. Kurat CF, Natter K, Petschnigg J, Wolinski H, Scheuringer K, Scholz H, et al.
880 Obese Yeast: Triglyceride Lipolysis Is Functionally Conserved from Mammals to
881 Yeast *. J Biol Chem. 2006;281: 491–500. doi:10.1074/jbc.M508414200

882 73. Zimmermann R, Strauss JG, Haemmerle G, Schoiswohl G, Birner-Gruenberger R,
883 Riederer M, et al. Fat Mobilization in Adipose Tissue Is Promoted by Adipose
884 Triglyceride Lipase. Science. 2004;306: 1383–1386.
885 doi:10.1126/science.1100747

886 74. Attané C, Peyot M-L, Lussier R, Poursharifi P, Zhao S, Zhang D, et al. A beta cell
887 ATGL-lipolysis/adipose tissue axis controls energy homeostasis and body weight
888 via insulin secretion in mice. Diabetologia. 2016;59: 2654–2663.
889 doi:10.1007/s00125-016-4105-2

890 75. Lee JH, Kong J, Jang JY, Han JS, Ji Y, Lee J, et al. Lipid Droplet Protein LID-1
891 Mediates ATGL-1-Dependent Lipolysis during Fasting in Caenorhabditis elegans.
892 Mol Cell Biol. 2014;34: 4165–4176. doi:10.1128/MCB.00722-14

893 76. Tuohetahuntila M, Molenaar MR, Spee B, Brouwers JF, Houweling M, Vaandrager
894 AB, et al. ATGL and DGAT1 are involved in the turnover of newly synthesized
895 triacylglycerols in hepatic stellate cells. J Lipid Res. 2016;57: 1162–1174.
896 doi:10.1194/jlr.M066415

897 77. Men TT, Thanh DNV, Yamaguchi M, Suzuki T, Hattori G, Arii M, et al. A *Drosophila*
898 Model for Screening Antiobesity Agents. BioMed Res Int. 2016;2016: 1–10.
899 doi:10.1155/2016/6293163

900 78. Li H, Janssens J, Waegeneer MD, Kolluru SS, Davie K, Gardeux V, et al. Fly Cell
901 Atlas: a single-cell transcriptomic atlas of the adult fruit fly. bioRxiv; 2021. p.
902 2021.07.04.451050. doi:10.1101/2021.07.04.451050

903 79. Xu T, Rubin GM. Analysis of genetic mosaics in developing and adult Drosophila
904 tissues. Development. 1993;117: 1223–1237.

905 80. Kim N, Nakamura H, Masaki H, Kumasawa K, Hirano K, Kimura T. Effect of lipid
906 metabolism on male fertility. Biochem Biophys Res Commun. 2017;485: 686–692.
907 doi:10.1016/j.bbrc.2017.02.103

908 81. Lasko PF, Ashburner M. The product of the Drosophila gene vasa is very similar to
909 eukaryotic initiation factor-4A. Nature. 1988;335: 611–617. doi:10.1038/335611a0

910 82. Resende LPF, Boyle M, Tran D, Fellner T, Jones DL. Headcase Promotes Cell
911 Survival and Niche Maintenance in the Drosophila Testis. Bökel C, editor. PLoS
912 ONE. 2013;8: e68026. doi:10.1371/journal.pone.0068026

913 83. Kiger AA, White-Cooper H, Fuller MT. Somatic support cells restrict germline stem
914 cell self-renewal and promote differentiation. Nature. 2000;407: 750–754.
915 doi:10.1038/35037606

916 84. Lin TY, Viswanathan S, Wood C, Wilson PG, Wolf N, Fuller MT. Coordinate
917 developmental control of the meiotic cell cycle and spermatid differentiation in
918 Drosophila males. Development. 1996;122: 1331–1341.

919 85. Eichmann TO, Kumari M, Haas JT, Farese RV, Zimmermann R, Lass A, et al.
920 Studies on the substrate and stereo/regioselectivity of adipose triglyceride lipase,
921 hormone-sensitive lipase, and diacylglycerol-O-acyltransferases. J Biol Chem.
922 2012;287: 41446–41457. doi:10.1074/jbc.M112.400416

923 86. Schweiger M, Schreiber R, Haemmerle G, Lass A, Fledelius C, Jacobsen P, et al.
924 Adipose Triglyceride Lipase and Hormone-sensitive Lipase Are the Major
925 Enzymes in Adipose Tissue Triacylglycerol Catabolism *. J Biol Chem. 2006;281:
926 40236–40241. doi:10.1074/jbc.M608048200

927 87. Missaglia S, Maggi L, Mora M, Gibertini S, Blasevich F, Agostoni P, et al. Late
928 onset of neutral lipid storage disease due to novel PNPLA2 mutations causing
929 total loss of lipase activity in a patient with myopathy and slight cardiac
930 involvement. Neuromuscul Disord. 2017;27: 481–486.
931 doi:10.1016/j.nmd.2017.01.011

932 88. Williams ML, Coleman RA, Placezk D, Grunfeld C. Neutral lipid storage disease: a
933 possible functional defect in phospholipid-linked triacylglycerol metabolism.
934 Biochim Biophys Acta BBA - Mol Basis Dis. 1991;1096: 162–169.
935 doi:10.1016/0925-4439(91)90055-E

936 89. Yang L, Liang J, Lam SM, Yavuz A, Shui G, Ding M, et al. Neuronal lipolysis
937 participates in PUFA-mediated neural function and neurodegeneration. EMBO
938 Rep. 2020;21. doi:10.15252/embr.202050214

939 90. Nazario-Yepiz NO, Fernández Sobaberas J, Lyman R, Campbell MR, Shankar V,
940 Anholt RRH, et al. Physiological and metabolomic consequences of reduced
941 expression of the Drosophila brummer triglyceride Lipase. Melkani GC, editor.
942 PLOS ONE. 2021;16: e0255198. doi:10.1371/journal.pone.0255198

943 91. Giedt MS, Thomalla JM, Johnson MR, Lai ZW, Tootle TL, Welte MA. Adipose
944 triglyceride lipase promotes prostaglandin-dependent actin remodeling by

945 regulating substrate release from lipid droplets. Cell Biology; 2021 Aug.
946 doi:10.1101/2021.08.02.454724

947 92. Beller M, Bulankina AV, Hsiao H-H, Urlaub H, Jäckle H, Kühnlein RP. PERILIPIN-
948 Dependent Control of Lipid Droplet Structure and Fat Storage in Drosophila. Cell
949 Metab. 2010;12: 521–532. doi:10.1016/j.cmet.2010.10.001

950 93. Buszczak M, Lu X, Segraves WA, Chang TY, Cooley L. Mutations in the midway
951 Gene Disrupt a Drosophila Acyl Coenzyme A: Diacylglycerol Acyltransferase.
952 Genetics. 2002;160: 1511–1518.

953 94. Martínez BA, Hoyle RG, Yeudall S, Granade ME, Harris TE, Castle JD, et al. Innate
954 immune signaling in Drosophila shifts anabolic lipid metabolism from triglyceride
955 storage to phospholipid synthesis to support immune function. PLOS Genet.
956 2020;16: e1009192. doi:10.1371/journal.pgen.1009192

957 95. Freeman DA, Ascoli M. Studies on the source of cholesterol used for steroid
958 biosynthesis in cultured Leydig tumor cells. J Biol Chem. 1982;257: 14231–14238.

959 96. Wang F, Chen Z, Ren X, Tian Y, Wang F, Liu C, et al. Hormone-sensitive lipase
960 deficiency alters gene expression and cholesterol content of mouse testis.
961 Reproduction. 2017;153: 175–185. doi:10.1530/REP-16-0484

962 97. Walther TC, Farese RV. Lipid droplets and cellular lipid metabolism. Annu Rev
963 Biochem. 2012;81: 687–714. doi:10.1146/annurev-biochem-061009-102430

964 98. Olzmann JA, Carvalho P. Dynamics and functions of lipid droplets. Nat Rev Mol
965 Cell Biol. 2019;20: 137–155. doi:10.1038/s41580-018-0085-z

966 99. Birse RT, Choi J, Reardon K, Rodriguez J, Graham S, Diop S, et al. High-fat-diet-
967 induced obesity and heart dysfunction are regulated by the TOR pathway in
968 Drosophila. Cell Metab. 2010;12: 533–44. doi:10.1016/j.cmet.2010.09.014

969 100. Molaei M, Vandehoef C, Karpac J. NF-κB Shapes Metabolic Adaptation by
970 Attenuating Foxo-Mediated Lipolysis in Drosophila. Dev Cell. 2019;49: 802-
971 810.e6. doi:10.1016/j.devcel.2019.04.009

972 101. Alic N, Andrews TD, Giannakou ME, Papatheodorou I, Slack C, Hoddinott MP, et
973 al. Genome-wide dFOXO targets and topology of the transcriptomic response to
974 stress and insulin signalling. Mol Syst Biol. 2011;7: 502. doi:10.1038/msb.2011.36

975 102. Junger MA, Rintelen F, Stocker H, Wasserman JD, Vegh M, Radimerski T, et al.
976 The Drosophila forkhead transcription factor FOXO mediates the reduction in cell
977 number associated with reduced insulin signaling. J Biol. 2003;2: 20.
978 doi:10.1186/1475-4924-2-20

979 103. Zinke I, Schutz CS, Katzenberger JD, Bauer M, Pankratz MJ. Nutrient control of
980 gene expression in Drosophila: microarray analysis of starvation and sugar-
981 dependent response. EMBO J. 2002;21: 6162–73.

982 104. Puig O, Tjian R. Transcriptional feedback control of insulin receptor by
983 dFOXO/FOXO1. Genes Dev. 2005;19: 2435–2446. doi:10.1101/gad.1340505

984 105. Kang P, Chang K, Liu Y, Bouska M, Birnbaum A, Karashchuk G, et al. Drosophila
985 Kruppel homolog 1 represses lipolysis through interaction with dFOXO. Sci Rep.
986 2017;7: 16369. doi:10.1038/s41598-017-16638-1

987 106. Bartz R, Zehmer JK, Zhu M, Chen Y, Serrero G, Zhao Y, et al. Dynamic activity of
988 lipid droplets: protein phosphorylation and GTP-mediated protein translocation. J
989 Proteome Res. 2007;6: 3256–3265. doi:10.1021/pr070158j

990 107. Pagnon J, Matzaris M, Stark R, Meex RCR, Macaulay SL, Brown W, et al.
991 Identification and functional characterization of protein kinase A phosphorylation
992 sites in the major lipolytic protein, adipose triglyceride lipase. Endocrinology.
993 2012;153: 4278–4289. doi:10.1210/en.2012-1127

994 108. Narbonne P, Roy R. Caenorhabditis elegans dauers need LKB1/AMPK to ration
995 lipid reserves and ensure long-term survival. Nature. 2009;457: 210–214.
996 doi:10.1038/nature07536

997 109. Ahmadian M, Abbott MJ, Tang T, Hudak CSS, Kim Y, Bruss M, et al.
998 Desnutrin/ATGL is regulated by AMPK and is required for a brown adipose
999 phenotype. Cell Metab. 2011;13: 739–748. doi:10.1016/j.cmet.2011.05.002

1000 110. Amoyel M, Hillion K-H, Margolis SR, Bach EA. Somatic stem cell differentiation is
1001 regulated by PI3K/Tor signaling in response to local cues. Dev Camb Engl.
1002 2016;143: 3914–3925. doi:10.1242/dev.139782

1003 111. Amoyel M, Simons BD, Bach EA. Neutral competition of stem cells is skewed by
1004 proliferative changes downstream of Hh and Hpo. EMBO J. 2014;33: 2295–2313.
1005 doi:10.15252/embj.201387500

1006 112. Ueishi S, Shimizu H, H. Inoue Y. Male Germline Stem Cell Division and
1007 Spermatocyte Growth Require Insulin Signaling in Drosophila. Cell Struct Funct.
1008 2009;34: 61–69. doi:10.1247/csf.08042

1009 113. Hof-Michel S, Cigoja L, Huhn S, Bökel C. Innate immune signalling drives loser
1010 cell elimination during stem cell competition in the *Drosophila* testis.
1011 Developmental Biology; 2020 Mar. doi:10.1101/2020.03.05.979161

1012 114. Couderc J-L, Richard G, Vachias C, Mirouse V. Drosophila LKB1 is required for
1013 the assembly of the polarized actin structure that allows spermatid
1014 individualization. White-Cooper H, editor. PLOS ONE. 2017;12: e0182279.
1015 doi:10.1371/journal.pone.0182279

1016 115. Steinhauer J, Statman B, Fagan JK, Borck J, Surabhi S, Yarikipati P, et al.
1017 Combover interacts with the axonemal component Rsp3 and is required for
1018 Drosophila sperm individualization. Dev Camb Engl. 2019;146: dev179275.
1019 doi:10.1242/dev.179275

1020 116. Tartarin P, Guibert E, Touré A, Ouiste C, Leclerc J, Sanz N, et al. Inactivation of
1021 AMPKα1 induces asthenozoospermia and alters spermatozoa morphology.
1022 Endocrinology. 2012;153: 3468–3481. doi:10.1210/en.2011-1911

1023 117. Martin-Hidalgo D, Hurtado de Llera A, Calle-Guisado V, Gonzalez-Fernandez L,
1024 Garcia-Marin L, Bragado MJ. AMPK Function in Mammalian Spermatozoa. Int J
1025 Mol Sci. 2018;19: 3293. doi:10.3390/ijms19113293

1026 118. Pitetti J-L, Calvel P, Zimmermann C, Conne B, Papaioannou MD, Aubry F, et al.
1027 An Essential Role for Insulin and IGF1 Receptors in Regulating Sertoli Cell
1028 Proliferation, Testis Size, and FSH Action in Mice. Mol Endocrinol. 2013;27: 814–
1029 827. doi:10.1210/me.2012-1258

1030 119. Thurmond J, Goodman JL, Strelets VB, Attrill H, Gramates LS, Marygold SJ, et al.
1031 FlyBase 2.0: the next generation. Nucleic Acids Res. 2018;47: D759–D765.
1032 doi:10.1093/nar/gky1003

1033 120. White-Cooper H. Spermatogenesis. In: Henderson DS, editor. Drosophila
1034 Cytogenetics Protocols. Totowa, NJ: Humana Press; 2004. pp. 45–75.
1035 doi:10.1385/1-59259-665-7:45

1036 121. Fabian L, Brill JA. Drosophila spermiogenesis. Spermatogenesis. 2012;2: 197–
1037 212. doi:10.4161/spmg.21798

1038 122. Schindelin J, Arganda-Carreras I, Frise E, Kaynig V, Longair M, Pietzsch T, et al.
1039 Fiji: an open-source platform for biological-image analysis. Nat Methods. 2012;9:
1040 676–682. doi:10.1038/nmeth.2019

1041 123. Yu H, Villanueva N, Bittar T, Arsenault E, Labonté B, Huan T. Parallel
1042 metabolomics and lipidomics enables the comprehensive study of mouse brain
1043 regional metabolite and lipid patterns. Anal Chim Acta. 2020;1136: 168–177.
1044 doi:10.1016/j.aca.2020.09.051

1045 124. Tsugawa H, Cajka T, Kind T, Ma Y, Higgins B, Ikeda K, et al. MS-DIAL: data-
1046 independent MS/MS deconvolution for comprehensive metabolome analysis. Nat
1047 Methods. 2015;12: 523–526. doi:10.1038/nmeth.3393

1048 125. Yu H, Huan T. Patterned Signal Ratio Biases in Mass Spectrometry-Based
1049 Quantitative Metabolomics. Anal Chem. 2021;93: 2254–2262.
1050 doi:10.1021/acs.analchem.0c04113

1051

1052
1053

1054

Figure 1 – Lipid droplets are present in early-stage somatic and germline cells.

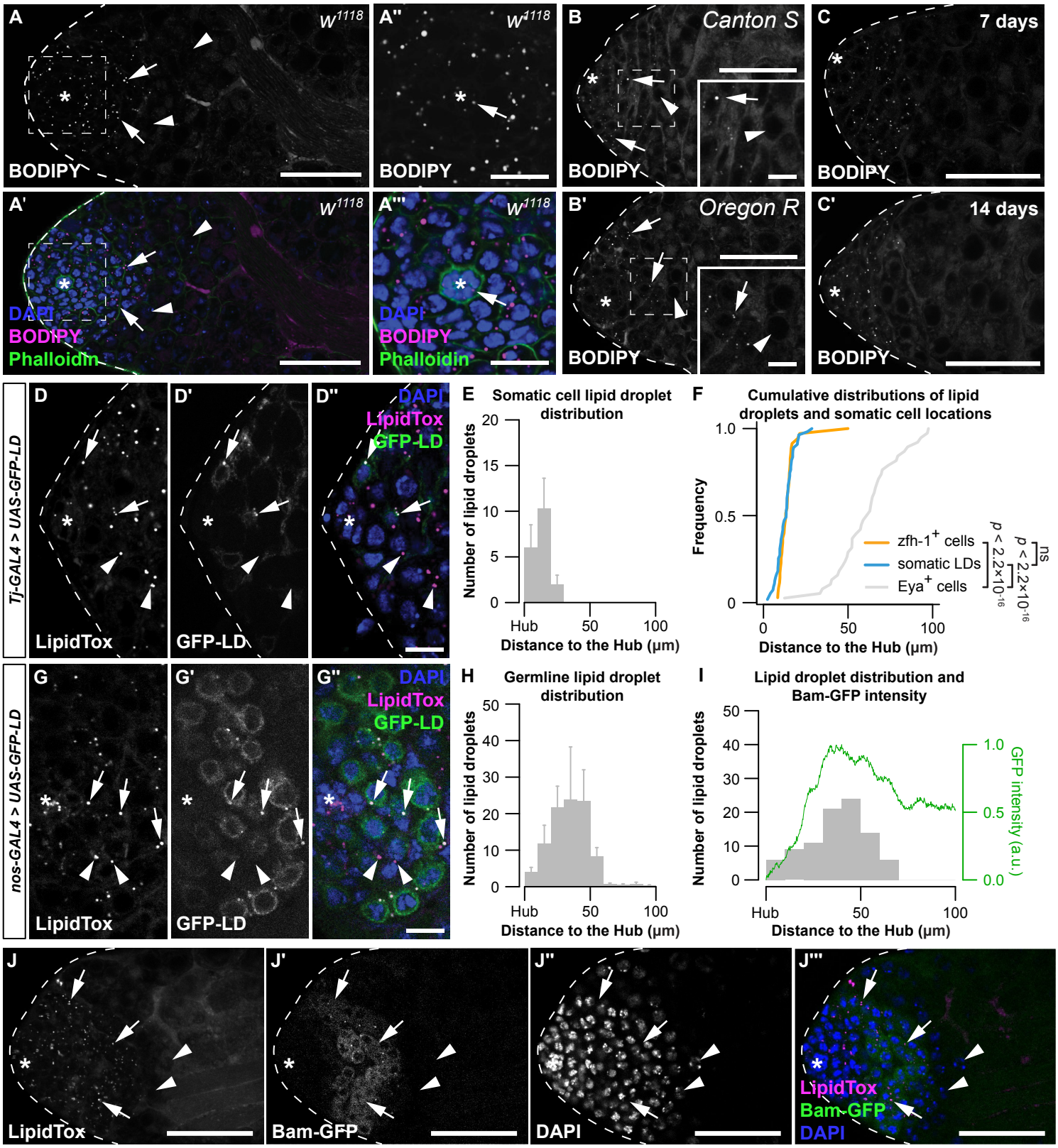

Figure 2 – *brummer* regulates testis lipid droplets in a cell-autonomous manner.

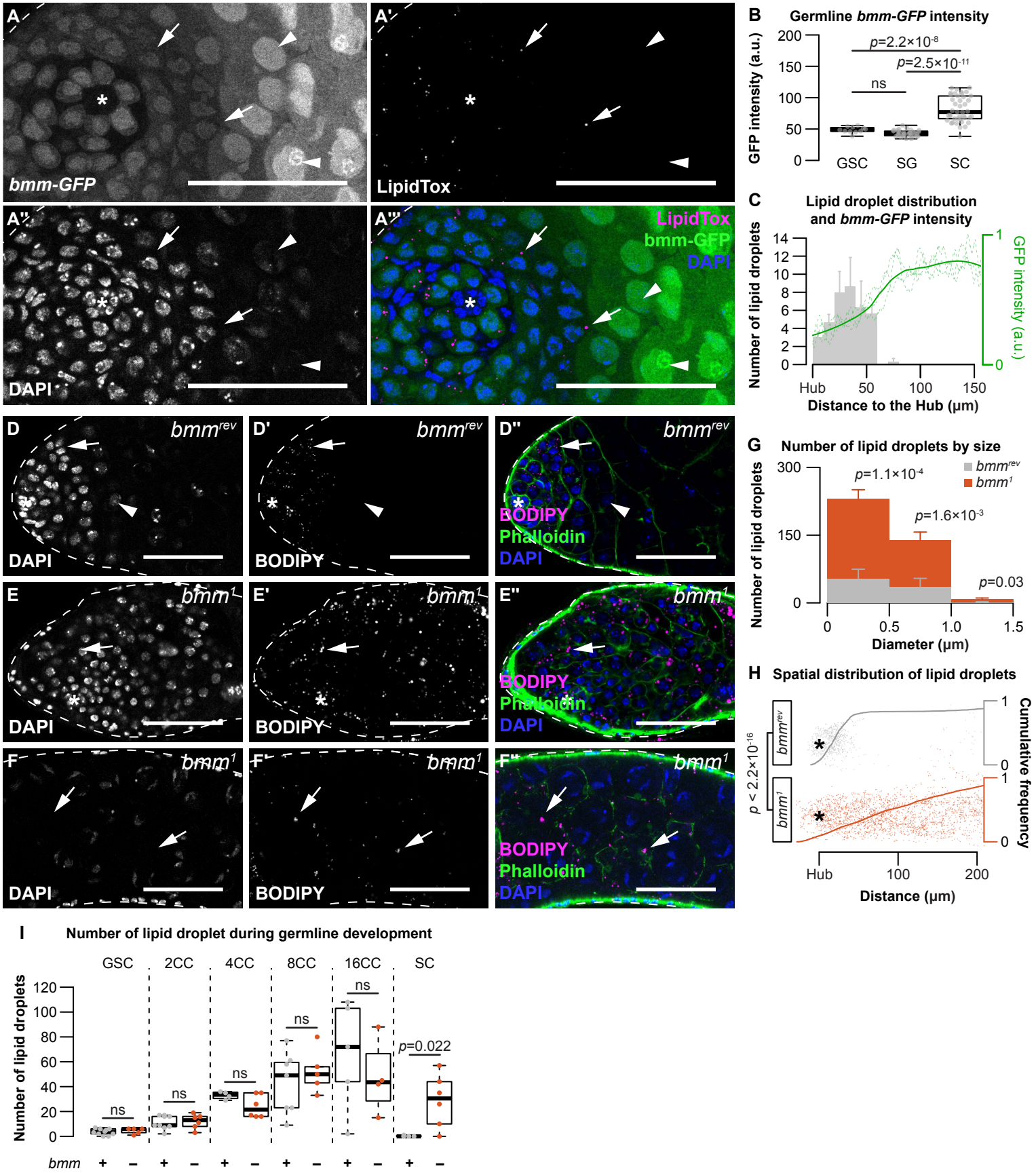

Figure 3 – A cell-autonomous role of *brummer* in regulating spermatogenesis.

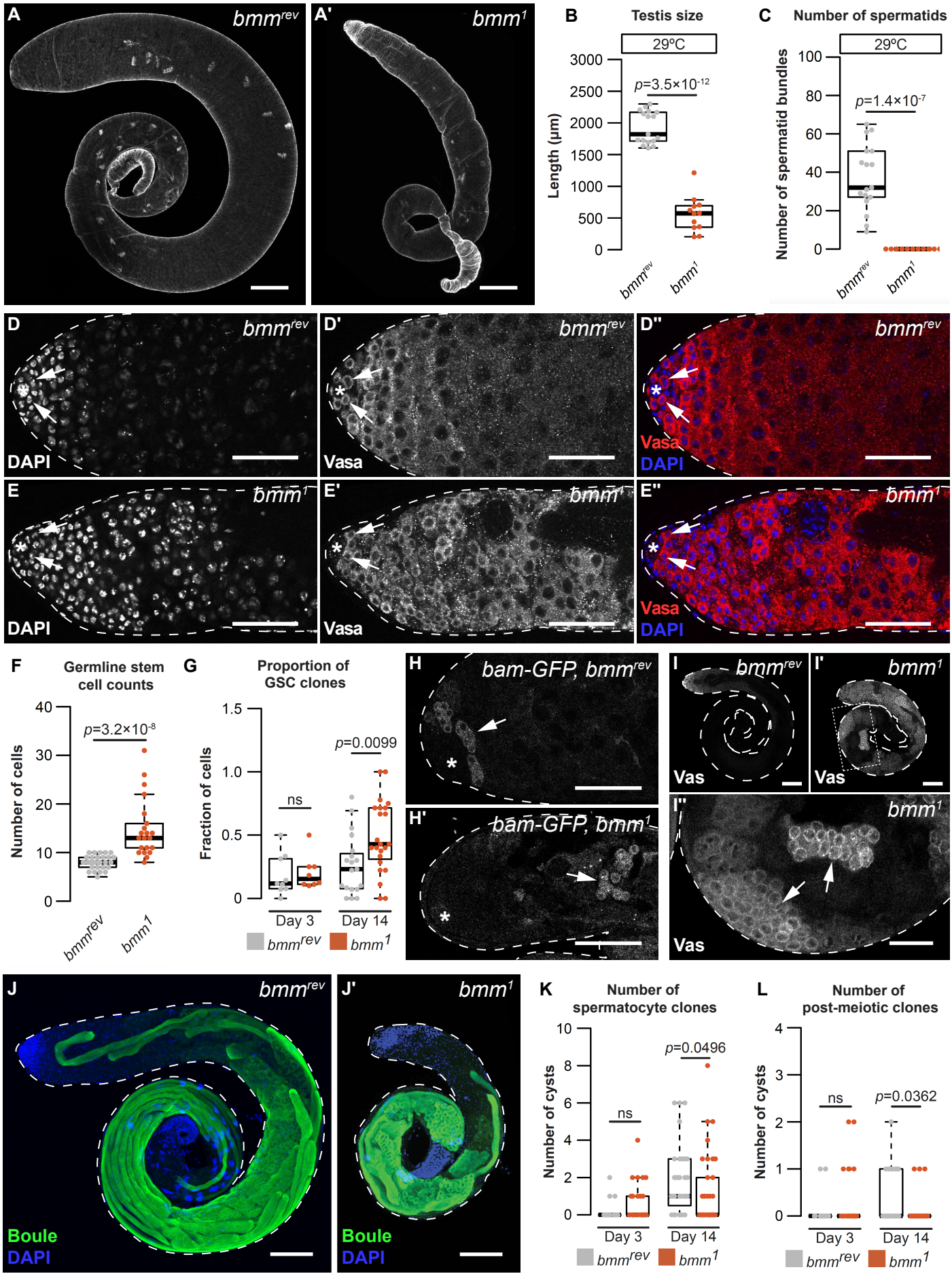

Figure 4 – Loss of *brummer* disrupts triglyceride homeostasis and leads to spermatogenic defects.

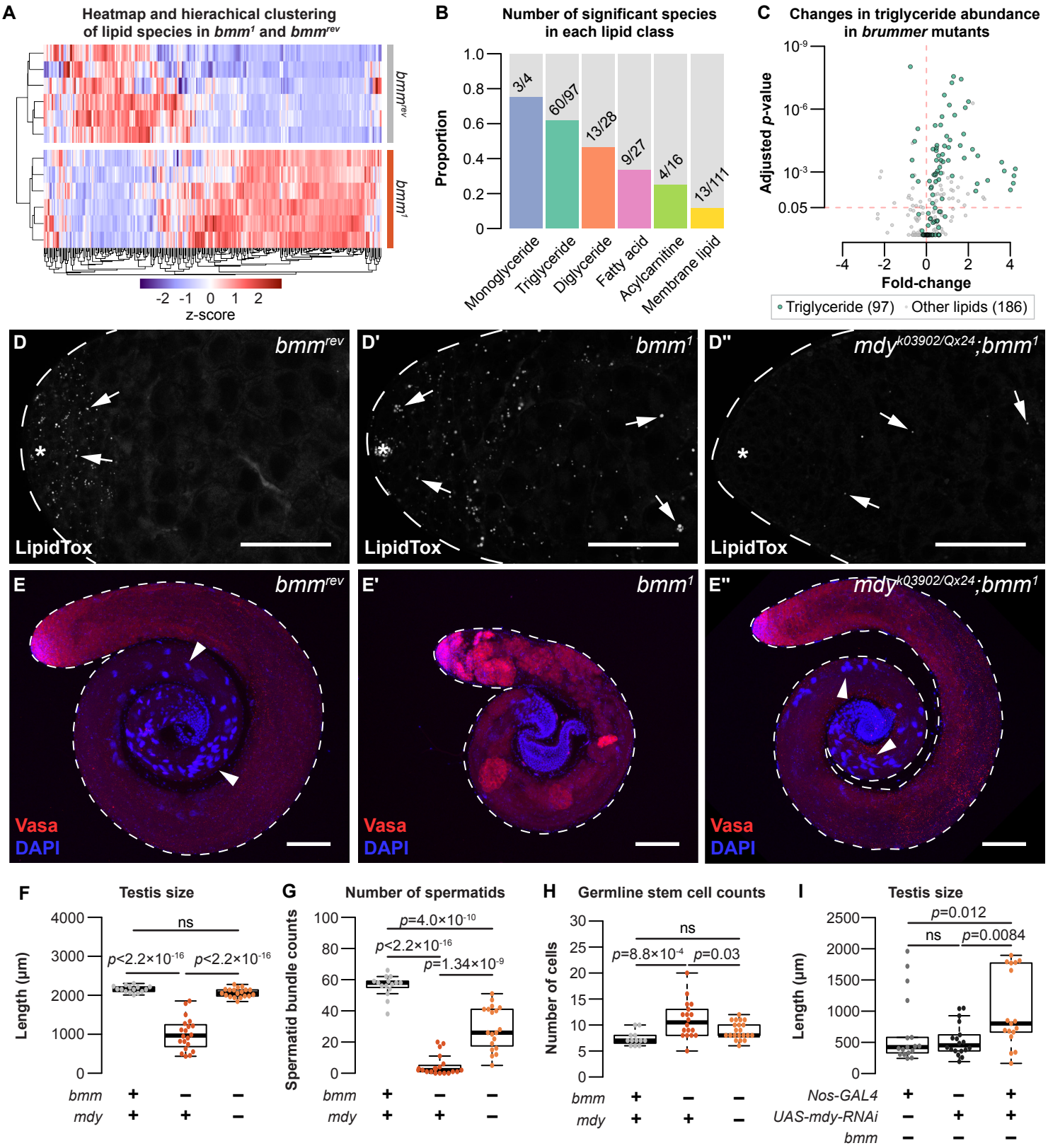

Supplemental Figure 1 – Cholesterol is absent from testis lipid droplets.

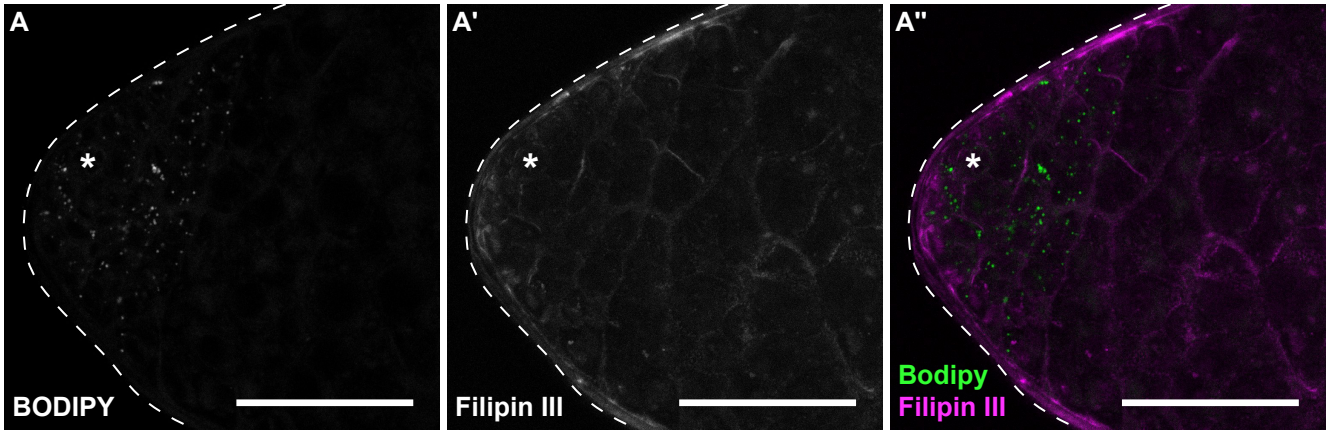

Supplemental Figure 2 – *brummer* regulates testis lipid droplets in a cell-autonomous manner.

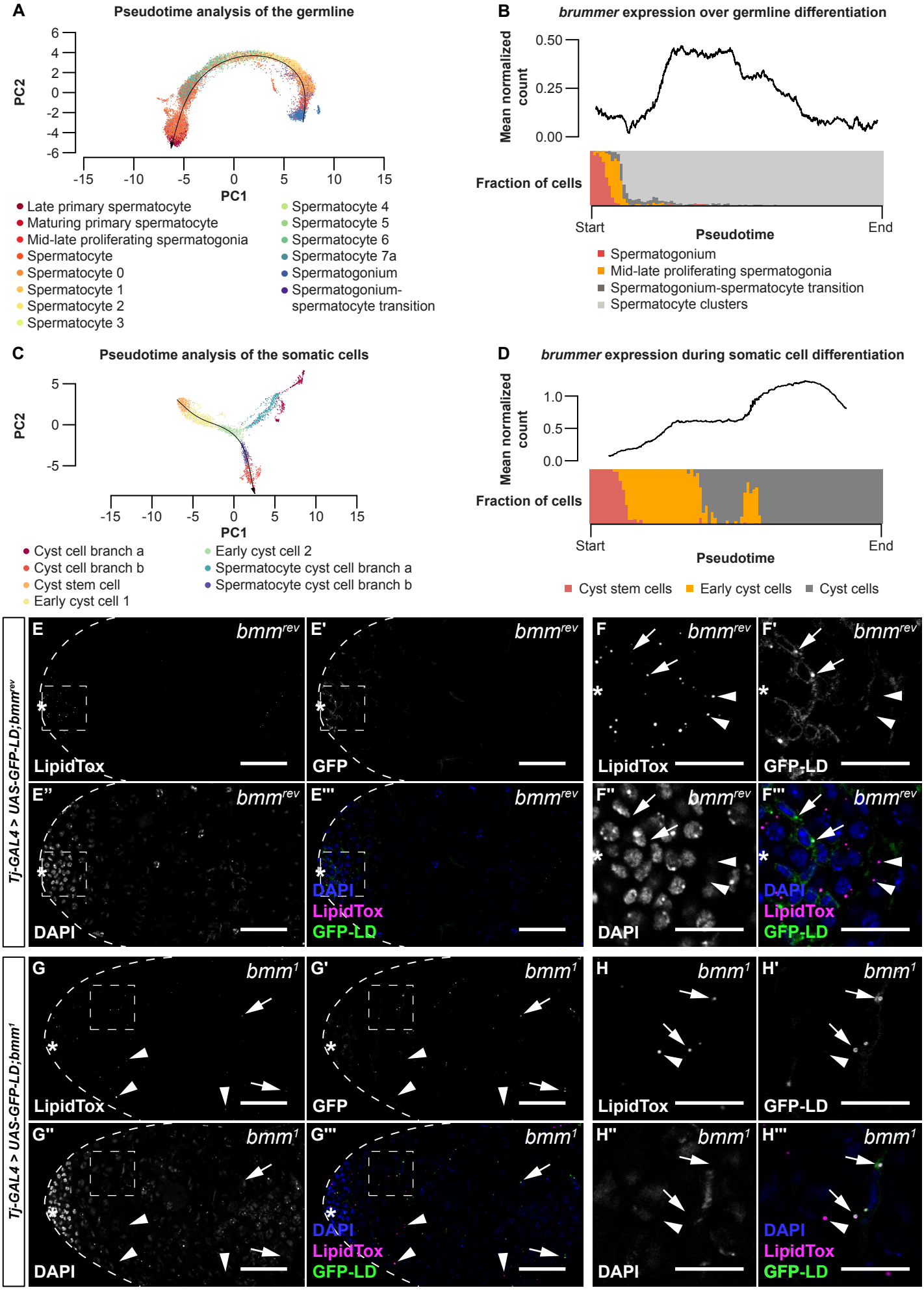

Supplemental Figure 3 – Additional characterization of testis development and spermatogenesis in animals lacking *brummer*.

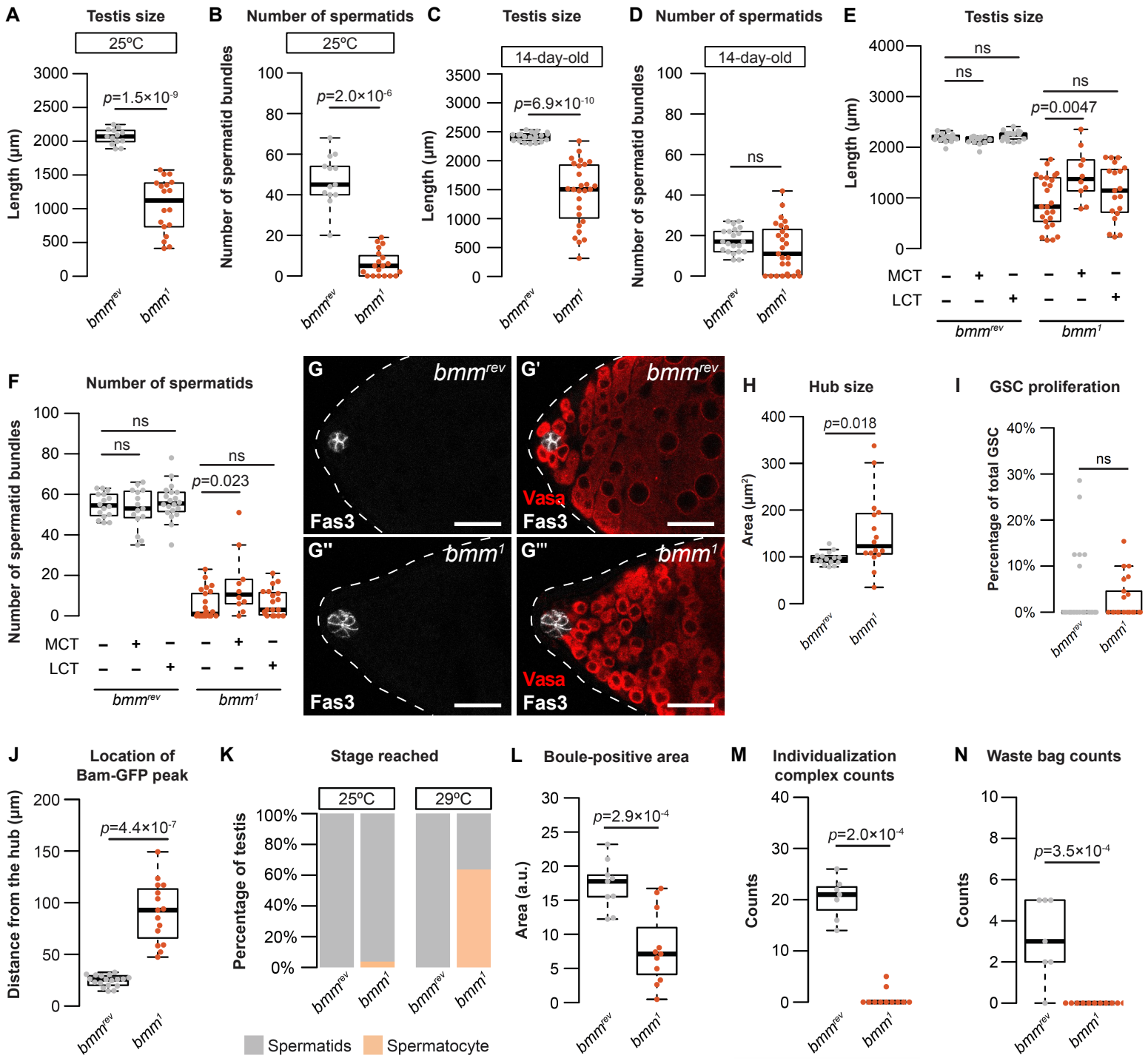
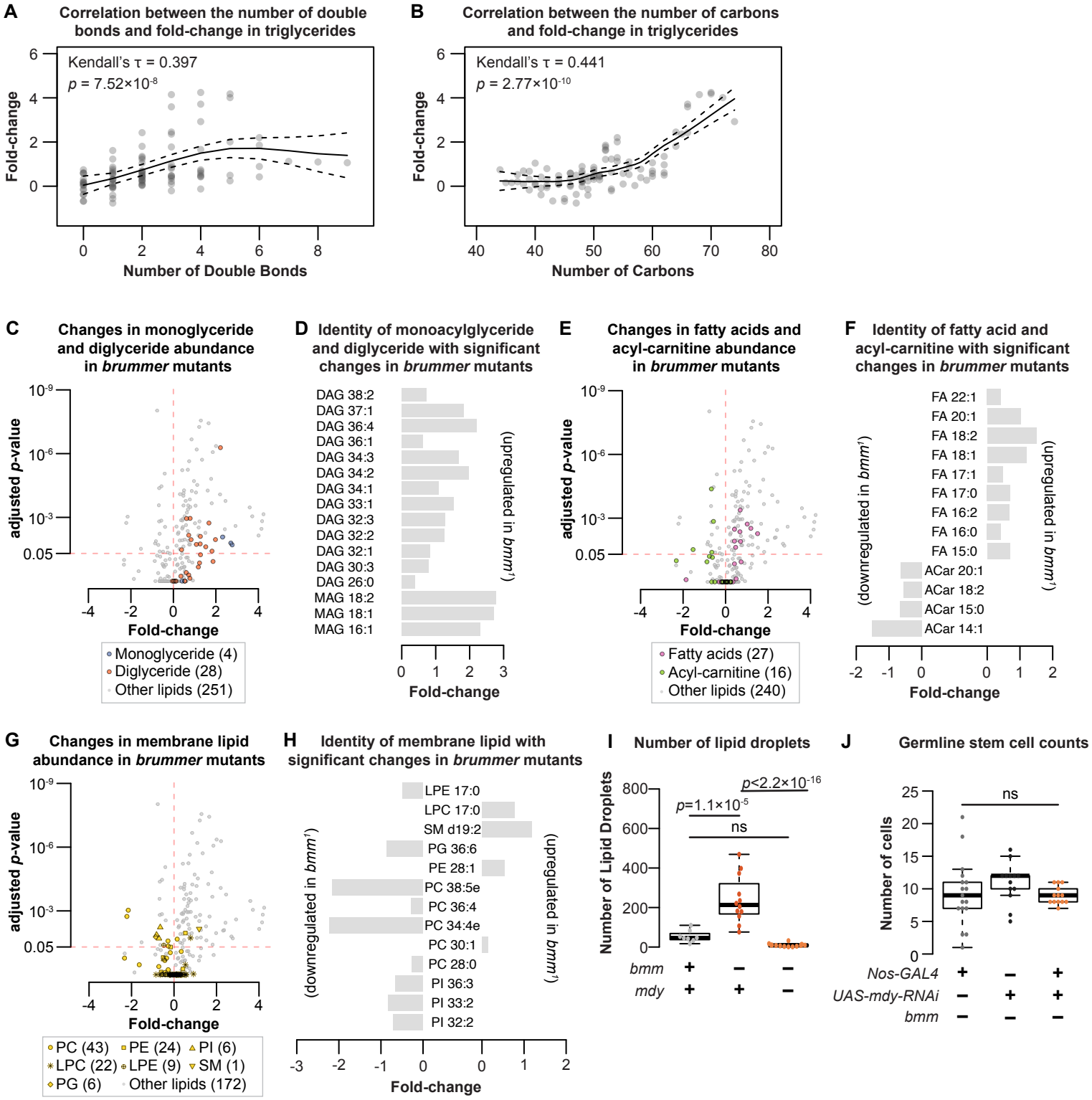
Supplemental Figure 4 – Lipidomic analysis of animals lacking *brummer*.